Accepted Manuscript

Early Cretaceous (~140Ma) aluminous A-type granites in the Tethyan Himalaya, Tibet: Products of crust-mantle interaction during lithospheric extension

Lin Ma, Andrew C. Kerr, Qiang Wang, Zi-Qi Jiang, Wan-Long Hu
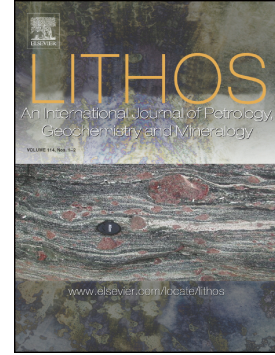
Please cite this article as: Lin Ma, Andrew C. Kerr, Qiang Wang, Zi-Qi Jiang, Wan-Long Hu , Early Cretaceous (~140Ma) aluminous A-type granites in the Tethyan Himalaya, Tibet: Products of crust-mantle interaction during lithospheric extension. The address for the corresponding author was captured as affiliation for all authors. Please check if appropriate. Lithos(2017), doi:10.1016/j.lithos.2017.11.023

Early Cretaceous (~140 Ma) aluminous A-type granites in the Tethyan Himalaya, Tibet: products of crust-mantle interaction during lithospheric extension

Lin Ma[1, 2*], Andrew C. Kerr[2], Qiang Wang[1, 3, 4*], Zi-Qi Jiang[1, 5], Wan-Long Hu[1, 4]

[1] State Key Laboratory of Isotope Geochemistry, Guangzhou Institute of Geochemistry, Chinese Academy of Sciences, Guangzhou 510640, China

[2] School of Earth and Ocean Sciences, Cardiff University, Cardiff, Wales CF10 3AT, United Kingdom

[3] CAS Centre for Excellence in Tibetan Plateau Earth Sciences, Beijing 100101, China

[4] University of Chinese Academy of Sciences, Beijing 100049, China

[5] School of Earth Science, Guilin University of Technology, Guilin, 541004, China

*Corresponding authors

Telephone: + 86 20 85292337 (L. Ma); +86 20 85290277 (Q. Wang). Fax: +86 20 85290277 (Q. Wang).

E-mail: malin@gig.ac.cn (L. Ma); wqiang@gig.ac.cn (Q. Wang)

Abstract

A-type granites have been the focus of considerable research due to their distinctive major- and trace-element signatures and tectonic significance. However, their petrogenesis, magmatic source and tectonic setting remain controversial, particularly for aluminous A-type granites. The earliest Cretaceous (ca. 140 Ma) Comei granite in the eastern Tethyan Himalaya is associated with coeval oceanic island basalt (OIB)-type mafic lava, and has A-type granite geochemical characteristics including high $10000 \times Ga/Al$ (up to 6), FeO^{total}/MgO (4.6–6.1) and $(Na_2O + K_2O)/Al_2O_3$ (0.50–0.61) ratios but low CaO (0.6–1.6 wt.%) and Na_2O (1.8–2.6 wt.%) contents. The Comei granite also has variable peraluminous compositions (A/CNK =1.00–1.36) along with zircon $\delta^{18}O$, $\varepsilon_{Nd}(t)$ and initial $^{87}Sr/^{86}Sr$ values of 8.2‰ to 9.3‰, -13.0 to -12.4 and 0.7238 to 0.7295, respectively. This range of compositions can be interpreted as the interaction between high-temperature upwelling OIB type basaltic magmas and a shallow crustal (< 5 kbar) metapelitic source. The Comei granite and coeval OIB type basaltic rock could represent the earliest stage (145–140 Ma) of a large igneous event in eastern Tethyan Himalaya, which may well have been triggered by pre-breakup lithospheric extension prior to the arrival of the Kerguelen plume head.

1. Introduction

A-type (alkaline, anhydrous and anorogenic) granites are defined as having high SiO$_2$, Na$_2$O+K$_2$O, Zr, Nb, Ga, Y and Ce, and low CaO and Sr contents and high Fe/Mg, Ga/Al ratios (Loiselle and Wones, 1979; Whalen et al., 1987) and can provide significant information on intraplate extensional or post-collisional magmatic processes within the continental lithosphere (e.g., Eby, 1990, 1992; Turner et al., 1992; Kerr and Fryer, 1993; Wang et al., 2010). Most A-type granites are peralkaline to metaluminous and a variety of processes have been proposed for their formation, such as fractionation of variously contaminated mantle-derived alkali basalt (e.g., Loiselle and Wones, 1979; Pearce et al., 1984; Eby, 1990, 1992; Turner et al., 1992), remelting of extracted F-rich lower crustal granulitic residue (e.g., Collins et al., 1982; Clemens et al., 1986;Whalen et al., 1987), low pressure melting of calc-alkaline rocks at upper crustal levels (Skjerlie and Johnston, 1993; Patiño Douce, 1997), and hybridization between anatectic granitic and mantle-derived mafic magmas (Bédard, 1990; Kerr and Fryer, 1993; Yang et al., 2006).

Aluminous A-type granites were identified by King et al. (1997) as a specific compositional type based on granites from the Lachlan Fold Belt (LFB) in southeastern Australia. These aluminous A-type granites have relatively high SiO$_2$, Fe^{total}/(Fe^{total}+Mg), K$_2$O, Ba, Al and low Sr, Ca with high temperatures of formation. Moreover, the common mafic minerals found in peralkaline A-type granites, including fayalite, hedenbergite, aegirine, ferrorichterite, riebeckite and arfvedsonite, have not been observed in the LFB aluminous A-type granites (King et al., 1997, 2001). Thus aluminous A-type granite was thought to have 'normal' H$_2$O contents that were similar to felsic I-type granite and, unlike the peralkaline A-type granite, did

3

not have an anhydrous origin (King et al., 1997). Aluminous A-type granite has higher zircon saturation temperatures than other granite types and is proposed to have formed by high temperature partial melting of an infracrustal source (King et al., 1997). However, nature of such a felsic infracrustal source and the tectonic setting of aluminous A-type granites are controversial. For example, a study in the Yangtze Block of South China suggested that aluminous A-type granite is most probably derived from a charnockite source heated by large-scale magmatic underplating, rather than a tonalite source (Zhao et al., 2008). Whereas, high zircon $\delta^{18}O$ (8.0‰– 9.8‰) and negative zircon $\varepsilon_{Hf}(t)$ (–6.2 to –2.3) for another A-type granite in South China indicates the reworking of old supracrustal rocks (Huang et al., 2011).

Early Cretaceous (ca.133 Ma) aluminous A-type dacite has also been found near Nagarze (Fig. 1b) intruding the Sangxiu Formation in the eastern Tethyan Himalaya (Zhu et al., 2005, 2007). These dacites have been proposed to have been derived from anatexis of ensialic continental crust with the melting triggered by the Kerguelen Plume (Zhu et al., 2005, 2007). In this paper, we present detailed geochronology, major and trace element, along with Sr–Nd and zircon O isotopic data for newly discovered peraluminous A-type granites from Comei in the eastern Tethyan Himalaya, Tibet (Fig. 1b, c). These data provide us with an excellent opportunity to constrain the sources, petrogenesis and tectonic setting of aluminous A-type granites, particularly the role of crust-mantle interaction. Our new data indicate that the Comei A-type granites were possibly generated by the interaction between coeval basaltic magmas and a crustal metapelitic source, and represent an earliest Cretaceous (145– 140 Ma) large-scale igneous event triggered by the pre-breakup lithospheric extension prior to the arrival of the Kerguelen plume head below the region now occupied by the eastern Tethyan Himalaya.

4

2. Geological background and petrographic characteristics

The Himalayan orogen resulted from Indian-Asian continental collision and represents the southernmost section of Tibetan Plateau (Yin and Harrison, 2000). The eastern and western syntaxis of the orogen are marked by the Namche Barwa and Nanga Parbat peaks, respectively (Yin, 2006), while the Indus-Yarlung Tsangpo Suture (IYTS) to the north and the Main Frontal Thrust (MFT) to the south define the extent of the orogen (Fig. 1a) (Yin and Harrison, 2000). From north to south, the Himalayan orogen comprises four broadly parallel east-trending geologic units (Fig. 1a): (1) the Tethyan Himalayan sequence, composed of Proterozoic to Eocene siliciclastic and carbonate sedimentary and volcanic rocks (Yin, 2006; Guo and Wilson, 2012; Liu et al., 2014, 2016); (2) the Higher Himalayan crystalline complex, comprising Paleoproterozoic to Ordovician gneisses and aplitic granites (Yin, 2006; Guo and Wilson, 2012); (3) the Lesser Himalayan sequence, composed of Proterozoic–Cambrian low-grade metasedimentary rocks (Guo and Wilson, 2012); and (4) the sub-Himalaya sequence, of Miocene–Pliocene foreland basin deposits (Yin, 2006; Liu et al., 2014). These four tectonostratigraphic units are separated by three north-dipping tectonic boundaries from north to south (Yin, 2006; Guo and Wilson, 2012): (1) the South Tibetan Detachment system (STDS), which is a late Oligocene to Miocene (25–12 Ma) normal fault between the Tethyan Himalayan and Higher Himalayan sequences; (2) the Main Central Thrust (MCT), which is interpreted as a shear zone along which the Higher Himalayan sequence was emplaced southward over the Lesser Himalayan sequence; and (3) the Main Boundary Thrust (MBT), which is defined as a thrust emplacing the Lesser Himalayan sequence

5

over the sub-Himalaya sequence (Fig. 1a).

The Himalayan orogen is characterised by two sub-parallel belts of Cenozoic leucogranites, namely the Higher Himalayan and Tethyan Himalayan leucogranites (e.g., Harrison et al., 1999; Wu et al., 2015) (Fig. 1a). The more southerly Higher Himalayan leucogranites form sheets, dykes, sills and laccolithic bodies that were emplaced along the South Tibetan Detachment System (Le Fort et al., 1987; Harrison et al., 1999; Guo and Wilson, 2012; Wu et al., 2015). The Tethyan Himalayan leucogranites to the north are typically exposed in the cores of the North Himalayan domes within the central Tethyan Himalayan physiographic region (~80 km north of the Higher Himalayan leucogranite belt) (King et al., 2011; Zeng et al., 2011; Liu et al., 2014, 2016; Wu et al., 2015). Previous research has shown that the Higher Himalayan leucogranites were generally emplaced in the latest Eocene–middle Miocene from 35 to 12 Ma (e.g., Coleman, 1998; Harrison et al., 1999; Guo and Wilson, 2012; Liu et al., 2014, 2016) while the Tethyan Himalayan leucogranites were primarily intruded between 45 and 7 Ma (e.g., Zhang et al., 2004; Ding et al., 2005; King et al., 2011; Zeng et al., 2011; Liu et al., 2014, 2016). Although most Himalayan leucogranites appear to have been generated by anatexis of the Higher Himalayan sequence (Harrison et al., 1999; Guo and Wilson, 2012), more recent research has indicated that some Eocene–Oligocene leucogranites with high Sr/Y in the Tethyan Himalaya were formed by melting of thickened lower crustal materials (amphibolite and eclogite) (Zeng et al., 2011; Hou et al., 2012; Liu et al., 2014).

In addition to the Cenozoic leucogranite belts, a possible Early Cretaceous large igneous province (LIP) covering an area of ~50000 km^2 has been identified in the eastern Tethyan Himalaya in southeastern Tibet (e.g., Zhu et al., 2009, 2013) (Fig. 1b).

This igneous province comprises basaltic lavas, mafic sills, dolerite dykes, gabbroic intrusions and granites together with subordinate layered ultramafic intrusions and silicic volcanic rocks (Zhong et al., 2005; Zhu et al., 2005, 2007, 2008, 2009, 2013; Jiang et al., 2006; Xia et al., 2014; Lv et al., 2016). Existing chronological data indicate that these igneous rocks were emplaced between 145–125 Ma with a possible peak of activity at 132 Ma (Zhong et al., 2005; Zhu et al., 2007, 2008, 2009; Jiang et al., 2006; Xia et al., 2014; Lv et al., 2016). U-Pb data of detrital zircons found in the Cretaceous to Paleocene sandstones also cluster between 142 Ma and 116 Ma in the Tethyan Himalayan unit (Hu et al., 2015).

Several models have been proposed for the formation of Tethyan Himalayan LIP: a) interaction between melts from the Kerguelen mantle plume head and the lithosphere of the northeastern margin of Greater India (e.g., Zhu et al., 2005, 2007, 2008, 2009); b) mantle melting caused by lithospheric thinning and consequent decompression melting during extension of the Neo-Tethyan passive continental margin (e.g., Zhong et al., 2005; Jiang et al., 2006, 2007) or breakup of Eastern Gondwana (Hu et al., 2010).

The Comei granite has been discovered within the Tethyan Himalayan LIP intruding the Jurassic Weimei formation which comprises sandy slate and siltstone. The granites are generally porphyritic (Fig. 2) and have medium- to fine-grained (3–20 mm) granular textures (Fig. 2). Like the A-type dacites reported in the Sangxiu Formation (Zhu et al., 2007), the Comei A-type granites are also shallow-level intrusions and this is evidenced by the presence of aplites, miarolitic cavities and some graphic intergrowths seen in thin section (Fig. 2). The phenocrysts in these granites mainly consist of quartz (30–35 vol.%), plagioclase (20–25 vol.%),

K-feldspar (25–30 vol.%) and muscovite (5 vol.%), with minor zircon, iron oxides and secondary chlorite (5–8 vol.%), calcite (3vol.%) and epidote (Fig. 2). The groundmass consists of fine quartz, plagioclase, K-feldspar, muscovite and secondary chlorite (Fig. 2). Plagioclase crystals in these granites are euhedral or subhedral (Fig. 2b). The vast majority of feldspars in the Comei granite are albites ($An_{0-8}Ab_{91-99}Or_{0-1}$) with minor alkali feldspar ($An_5Ab_{76}Or_{20}$). The presence of abundant crystal holes (Fig. 2f) suggests the presence of significant volatiles during magma crystallisation. Like the aluminous A-type granites in Lachlan Fold Belt (King et al., 1997) and northeastern China (Wu et al., 2002), the Comei granite lacks mafic minerals such as hedenbergite, aegirine, ferrorichterite that are commonly found in peralkaline A-type granites. In addition, the widespread occurrence of chlorite (Fig. 2d) indicates that the Comei granite experienced low grade greenschist facies metamorphism.

3. Analytical methods

The mineral compositions were analysed using a JXA–8230 electron microprobe at Key Laboratory of Mineralogy and Metallogeny (KLMM), Guangzhou Institute of Geochemistry (GIG), Chinese Academy of Sciences (CAS). The accelerating voltage was 15 kV with a specimen current of 3.0×10^{-8} A and a beam of 1 μm in diameter. See Huang et al. (2007) for more details.

Cathodoluminescence (CL) imaging of zircon was performed using a Mono CL^{3+} detector (Gatan, Pleasanton, CA, USA) attached to a field emission electron microscope (SUPRA 55 SAPPHIRE, ZEISS, Germany) at State Key Laboratory of Isotope Geochemistry (SKLaBIG) GIG CAS. Zircon U-Pb isotope dating of sample 09TB116-1 was conducted by a Cameca IMS-1280 secondary ion mass spectrometry

(SIMS) at the Institute of Geology and Geophysics (IGG) CAS. The standard zircon Plešovice (Sláma et al., 2008) and Qinghu (Li et al., 2013) were used to correct U–Th–Pb ratios and their absolute abundances, respectively. Concordia plots and weighted mean U–Pb ages with 2σ were processed using the Isoplot/Ex v.3.0 program (Ludwig, 2003). Four Qinghu zircon spots were analysed and yielded a mean age of 158.5 ± 2.4 Ma, which is within error of the recommended value of 159.5 ± 0.2 Ma (Li et al., 2013). The Plešovice zircon yielded a weighted $^{206}Pb/^{238}U$ age of 338.1 ± 3.1 Ma (2σ, MSWD = 0.2, n = 10), which is identical within error to the recommended $^{206}Pb/^{238}U$ age of 337.1 ± 0.4 Ma) (Sláma et al., 2008). The zircon U–Pb age data are presented in Supplementary Table A2.

U-Pb zircon dating (using LA-ICP-MS) of sample 11SN19-3 was performed using an Agilent 7500a ICPMS with a RESOlution M-50 laser-ablation system at KLMM GIG CAS. Laser ablation was set to a constant energy of 80 mJ and a pulse repetition rate of 8 Hz, with a spot size of 31 μm. Helium was used to carry ablated material to the Aglient 7500a ICP-MS. Element corrections were determined relative to standard glass NIST 610 (Pearce et al. 1997). During the study, the zircon standard Temora yielded a weighted mean $^{206}Pb/^{238}U$ age of 417.0 ± 3.0 Ma (2σ, MSWD = 0.001, n = 22), which is in within error of the recommended value of 416.8 ± 1.1 Ma (Black et al. 2003)

Rock samples were first examined by optical microscopy. Selected whole-rock samples were broken into small chips and cleaned ultrasonically in distilled water containing < 3% HNO_3 and washed with distilled water before being dried and handpicked to remove visible contamination. The rocks were powdered before analysis of major and trace elements, and Sr-Nd isotopes at SKLaBIG GIG CAS.

Major-element oxides were determined by a Rigaku RIX 2000 X-ray fluorescence spectrometer on fused glass beads with analytical uncertainties < 5% at SKLaBIG GIG CAS (Li et al., 2005). Trace elements were analysed by a Perkin–Elmer Sciex ELAN 6000 ICP-MS at SKLaBIG GIG CAS. Trace element data of reference materials (BHVO-2, GSR-1, GSR-2, GSR-3, SARM-4, AGV-2 and W-2a) and replicate samples are given in Supplementary Table A4. The relative standard deviations are < 3% for most element abundances in the reference materials.

Sr and Nd isotope analysis were performed using a MC–ICPMS at SKLaBIG, GIG–CAS. Analytical procedures are identical to those described by Wei et al. (2002) and Li et al. (2004). The NBS987 and the Shin Etsu JNdi–1 standard yielded a $^{87}Sr/^{86}Sr$ ratio of 0.710285 ± 15 (2σ) and a $^{143}Nd/^{144}Nd$ ratio of 0.512085 ± 10 (2σ), respectively. All measured $^{143}Nd/^{144}Nd$ and $^{86}Sr/^{88}Sr$ ratios were corrected to $^{146}Nd/^{144}Nd$ = 0.7219 and $^{86}Sr/^{88}Sr$ = 0.1194, respectively. BCR-2 and JB-3 were analysed as unknown samples and yielded $^{87}Sr/^{86}Sr$ and $^{143}Nd/^{144}Nd$ ratios of 0.705013 ± 18 (2σ, n=6), 0.703420 ± 23 (2σ, n=6), and 0.512628 ± 2 (2σ, n=6) and 0.513049 ± 10 (2σ, n=6), respectively. All these data are in good agreement with the recommended $^{87}Sr/^{86}Sr$ and $^{143}Nd/^{144}Nd$ ratios of 0.705000 ± 11 (Jweda et al., 2015), 0.703428 ± 10 (Okano et al., 1989), and 0.512637 ± 13 (Jweda et al., 2015) and 0.513035 ± 9 (Lizumi et al., 1995).

O isotopes in zircons were measured by a Cameca IMS-1280 SIMS at IGG CAS. Analytical procedures are similar to those described by Li et al. (2010). Twelve analyses of the Qinghu zircon standard yielded a weighted mean $\delta^{18}O$ of 5.38 ± 0.27‰, which is identical within error to the value of 5.39± 0.22‰ reported by Li et al. (2013).

4. Results

4.1 Zircon U–Pb geochronology

Two Comei granite samples (09TB116-1 and 11SN19-3) were selected for zircon U-Pb dating. Zircons in these samples have crystal lengths of ~50–200 μm and length/width ratios from 2:1 to 3:1. Zircon U–Pb isotopic data are given in Supplementary Table A2. Well-developed oscillatory zoning and high Th/U ratios indicate a magmatic origin of these zircons (Hoskin and Black, 2000). With the exception of some inherited zircons with old ages of 354 to 2533 Ma, U–Pb analyses on samples 09TB116-1 and 11SN19-3, yield concordant [207]Pb-corrected ages of 146–136 Ma (SIMS), and [206]Pb/[238]U ages of 143–136 Ma (LA-ICP-MS), with weighted mean ages of 139.7± 1.4 Ma (MSWD = 1.8, n = 22) and 139.6 ± 1.8 Ma (MSWD = 0.06, n = 12), respectively (Fig. 3; Supplementary Table A2). These ages indicate that the Comei granite was likely emplaced in the Early Cretaceous (ca. 140 Ma).

4.2 Major and trace element geochemistry

The Comei granite samples all have high SiO_2 (66.8–69.5 wt.%), K_2O (4.9–5.4 wt.%) and low CaO (0.6–1.6 wt.%), Na_2O (1.8–2.6 wt.%) and MgO (0.7–1.1 wt.%) contents with high FeO^{total}/MgO (4.6–6.1) ratios and variable peraluminous compositions (A/CNK = molecular $Al_2O_3/(CaO+Na_2O+K_2O)$ = 1.00–1.36) (Fig. 4; Table 1). Relatively lower Al_2O_3, CaO and TiO_2 and higher K_2O and Fe_2O_3 contents of the Comei granite samples clearly distinguish them from the Eocene lower crust-derived high Sr/Y granites (Zeng et al., 2011) (Fig. 4). In addition, they also have lower SiO_2, Al_2O_3 and Na_2O and higher MgO and TiO_2 contents than the

11

Oligocene–Miocene Himalayan leucogranites (e.g., Guo and Wilson, 2012).

The Comei granite samples have relatively high total rare earth element (REE) contents (373–851 ppm) and are characterised by moderately enriched light REE ($[La/Sm]_{CN}$ = 3.7–4.1) and relatively flat heavy REE ($[Gd/Yb]_{CN}$ = 1.9–2.4) chondrite-normalised patterns with moderately negative Eu anomalies (Eu/Eu* = $Eu_{CN}/(Sm_{CN}\times Gd_{CN})^{1/2}$ = 0.51–0.65) (Fig. 5a, Table 1). All Comei granite samples show nearly parallel REE patterns (Fig. 5a), suggesting a similar magma source and fractionation process. Sample 11SN17-1 shows the highest total REE (851 ppm) contents (Fig. 5a).

On primitive mantle normalised plots, the Comei granite samples are slightly enriched in many of the most incompatible elements including Th, U and Rb and are markedly depleted in Nb, Ta, Ti, Sr and Ba (Fig. 5a, Table 1). They possess significant negative Sr anomalies (Sr/Sr* = $2Sr_{PM}/(Ce_{PM}+Nd_{PM})$ = 0.04–0.09), negative Nb anomalies (Nb/Nb* = $2Nb_{PM}/(Th_{PM}+La_{PM})$ = 0.11–0.14) and negative Ti anomalies (Ti/Ti* = $2Ti_{PM}/(Sm_{PM}+Tb_{PM})$ = 0.14–0.18) (Fig. 5b). Moreover, the Comei granite samples also have significantly higher REEs and most incompatible element abundances compared to the Himalayan leucogranites and high Sr/Y granites (Fig. 5).

These geochemical characteristics, such as high Zr, Nb, Ce, Y and K_2O and low CaO contents with high FeO^{total}/MgO ratios, are consistent with the Early Cretaceous Comei granite being of A-type (e.g., Whalen et al., 1987; Eby, 1992; King et al, 1997). Furthermore, this granite is compositionally similar to the later (ca. 133 Ma) A-type dacites from the Sangxiu Formation in the Tethyan Himalaya (Zhu et al., 2005, 2007) (Fig. 6). The Early Cretaceous Comei granite samples also have relatively high 10000

✕Ga/Al ratios (2.4–6.0), again consistent with them being A-type granites (Fig. 6).

4.3 Sr–Nd isotope geochemistry

In this study, initial isotopic ratios of the Comei granite and literature data were calculated based on a mean formation age of 140 Ma. The whole rock Sr–Nd isotopic composition data of the Comei granite samples are given in Table 2. Overall the Comei granite exhibits uniform initial $^{87}Sr/^{86}Sr$ ratios (0.7253–0.7295) and negative $\varepsilon_{Nd}(t)$ values (-12.8 to -12.0) with Nd-isotope model ages (T_{DM}) ranging from 1.85 to 1.78 Ga (Fig. 7; Table 2). The Comei granite samples are more enriched in $^{87}Sr/^{86}Sr$ than those of the Eocene lower crust-derived high Sr/Y granitoids in the Tethyan Himalaya (e.g., Zeng et al., 2011; Hou et al., 2012; Liu et al., 2014) (Fig.7). However, their $\varepsilon_{Nd}(t)$ values are slightly higher than those of the Oligocene–Miocene leucogranites in the High Himalaya and Tethyan Himalaya (e.g., Guo and Wilson, 2012) (Fig.7).

4.4 Zircon O isotope geochemistry

In situ zircon O isotope data for sample 09TB116 are listed in Supplementary Table A2-1. Zircons from sample 09TB116 have high $\delta^{18}O$ values (8.2‰ to 9.3‰), which are markedly higher than those (5.3 ± 0.3‰) of igneous zircons in equilibrium with mantle magmas (Valley et al., 2005).

5. Discussion

5.1 Petrogenesis of the Comei granite

5.1.1 Effects of alteration and low-grade metamorphism

The widespread occurrence of secondary minerals (chlorite and epidote) and moderately high loss on ignition (LOI) values (1.98–3.27 wt.%) both suggest that the Comei granite underwent low grade metamorphism and alteration after emplacement. Hence, the potential effects of these processes on whole rock geochemistry need to be assessed before discussing their petrogenesis.

On primitive mantle-normalised trace-element diagrams, the Comei granite samples are characterised by sub-parallel patterns and uniform contents of REE and HFSE concentrations (Fig. 5b). These features are consistent with research which shows that in igneous rocks the REEs and HFSEs are relatively immobile during alteration and low-grade metamorphism (e.g., Bienvenu et al., 1990; Staudigel et al., 1996). Large ion lithophile elements (LILE: Rb, Ba, Sr, Th and U) are usually considered to be mobile during low-temperature alteration (Hawkesworth et al., 1997; Turner et al., 1997). However, in this study, with the exception of one sample (11SR17-1) with marked high trace element contents, nearly constant Rb, Th and U contents suggest that these elements were not significantly mobilised by sub-solidus processes (Fig. 8a, d, e).

The Comei granite samples also have relatively variable but narrow ranges of Ba, Sr contents and Sr isotope ratios (Fig. 8b, c, f), again suggesting a limited effect of alteration. Additionally, sub-parallel patterns and uniform contents of most LILE, HFSE and REE further indicate that the LILE are immobile in these granites during alteration and low-grade metamorphism. Furthermore, the Sr isotope signatures of the Comei granite are not only consistent with their enriched Nd isotope ratios, but are also similar to those of the Sangxiu A-type dacite (Zhu et al., 2007) and Himalayan leucogranites (Guo and Wilson, 2012) (Fig. 7). Therefore, the low-grade

metamorphism appears to have had an insignificant effect on the distribution of most elements in this study.

5.1.2 Hybrid source of the Comei granite

As mentioned above, the Comei are characterised by features of typical A-type granite including high SiO_2, Fe_2O_3, K_2O, Zr, Nb and low CaO contents with high FeO^T/MgO, $(Na_2O + K_2O)/Al_2O_3$ and Ga/Al ratios compared to calc-alkaline granites (Fig. 6). The high SiO_2 and low MgO contents of the Comei porphyritic granite (Fig. 4) suggests that it is unlikely to be derived directly from the mantle. Furthermore, the markedly high Zr, Nb, Ce, Y and Cr contents do not suggest that the Comei granite has undergone very significant fractionation (Fig. 6d, Table 1) since, during fractionation, granitic magma will decrease its concentrations of Cr, Ni, Co, Sr, Ba, Zr and other trace elements (Gelman et al., 2014; Lee and Morton, 2015; Wu et al., 2017).

In addition, the enrichment of the Comei porphyritic granite in K, Rb, and Th along with high initial $^{87}Sr/^{86}Sr$ ratios and low $\varepsilon_{Nd}(t)$ values strongly indicates an input from a crustal source (Fig. 5 and 7) as do the low Nb/U and high Ce/Y ratios that are similar to upper continental crust (Fig. 9). The low $\varepsilon_{Nd}(t)$ values and ancient Nd model ages (1.78–1.85 Ga) of the Comei porphyritic granite samples are also both similar to those of the metasediment-derived Himalayan leucogranites (e.g., Guo and Wilson, 2012), which further supports a upper crustal source.

The Comei granite samples have much higher zircon $\delta^{18}O$ values (8.2‰–9.3‰) (Supplementary Table A2). Magmatic zircon is able to preserve the magmatic O isotope ratio (Peck et al., 2003). Thus, so high zircon $\delta^{18}O$ values in the Comei granite, equivalent to whole-rock values of 9.8 ‰–11.0 ‰ (based on the equation of Valley et

al., 2005), require a source contribution of supracrustal components (Valley et al., 2005; Huang et al., 2011). The high $\delta^{18}O$ and evolved isotope compositions of the Comei granite samples most likely fingerprint the source from which the magmas were derived, indicating that it was principally of supracrustal origin.

Altherr et al. (2000) and Altherr and Siebel (2002) summarised the experimental data for common crustal melts. Using this compilation, the Comei granite with its low $CaO/(MgO+FeO^T)$ and high A/CNK (1.02–1.36) ratios are consistent with a metapelitic (MP) source, but differ substantially from melts of metagraywacke (MGW), meta-andesite (MA) and metabasalt (MB) (Fig. 10). In addition, Nd model ages can be integrated with Sr isotope data to constrain the Rb/Sr ratio of the granite source (Inger and Harris, 1993). Rb/Sr ratios will be increased by intracrustal processes such as melting and sedimentary cycles (McDermott and Hawkesworth, 1990), and so this value represents a minimum that is time-integrated over a possible series of fractionation events. For the Comei granite, such calculations constrain the Rb/Sr ratio in its source to be >3.5, consistent with migmatites of the Higher Himalayan slab (Inger and Harris, 1993) and typical pelite Rb/Sr ratios of 3−6 (Harris et al., 1992). Thus, it seems probable that the Early Cretaceous Comei porphyritic granite was mainly derived from a Himalayan metapelitic source.

However, the Comei granite is unlikely to represent pure crustal melts. Experimental data indicate that such continental crustal melts are produced by incongruent dehydration-melting and are silica-rich, with SiO_2 contents $\geqslant 70$ wt.% (Patiño Douce, 1999). Thus, the relatively lower SiO_2 contents (68.1–69.5 wt.%) and slightly higher $\varepsilon_{Nd}(t)$ (-12.0 to -12.8) values of the Comei granite compared to those (70.6–75.3 wt.% and -14.4 to -18.4) of the Himalaya leucogranites (Fig. 7; Guo and

Wilson, 2012) likely suggest that a small amount of mantle-derived melt contributed to the Early Cretaceous Comei granite magmas. The lower SiO_2 contents (68.1–69.5 wt.%) than those (72.2–73.9 wt.%) of the lower crust-derived Yardoi I-type granites with similar MgO contents in Tethyan Himalaya (Zeng et al., 2011) also suggest that the lower SiO_2 contents of the Comei granite are not due to it having undergone less fractionation. In addition, the occurrence of coeval (145 Ma) oceanic island basalts (OIB) type basalts in Tethyan Himalaya (Zhu et al., 2008) and the relatively high MgO (0.70–1.07 wt.%) and Cr contents (77–218 ppm) of some of the Comei granite samples (Table 1) both support this inference. Therefore, it is likely that the Comei granite was derived from a hybrid source including mantle derived magmas and metapelite crustal melts.

In this study, the metasediment-derived Lhozhag leucogranites located the eastern Tethyan Himalaya have been selected to represent a possible crustal end-member of the Comei granite, given their similar geographic distribution and that they are the likely source of the High Himalaya crystalline complex (Guo and Wilson, 2012). This High Himalaya crystalline complex is generally considered to represent the basement rocks of the Tethyan Himalaya (Yin, 2006). In contrast, an alternative crustal end-member, such as high Sr/Y lower crust-derived granite in Tethyan Himalaya, extends to higher $\varepsilon_{Nd}(t)$ values and lower initial $^{87}Sr/^{86}Sr$ ratios than the Comei granite (Fig. 7) (Zeng et al., 2011; Liu et al., 2014), and so cannot represent their crustal end-member. Thus, we propose the involvement of felsic metapelite-derived melts represented by the Lhozhag leucogranites in the Tethyan Himalaya in the formation of the Comei granite.

Both the Early Cretaceous OIB- and normal mid-ocean ridge basalts

(N-MORB)-type basalt, dolerite and gabbro in the eastern Tethyan Himalaya are characterised by depleted LREE and incompatible elements (Zhu et al., 2008), which are clearly distinct from the compositions of the Comei granite. Furthermore, in order to model the observed Nd isotopic composition of the Comei granite, a contribution of ~40% N-MORB type mafic magma would be required Involvement of such a high percentage of mantle-derived magma cannot be reconciled with high SiO_2 and low MgO contents of the Comei granite. These indicate that N-MORB type mafic rocks are not suitable as a mafic end-member of the Early Cretaceous Comei granite, and the OIB type basalts are a more likely mantle-derived end-member.

Modelling of Sr–Nd isotope systematics with a variety of Nd content ratios (Nd_{mantle}/Nd_{crust} =1–40) between the Tethyan Himalayan OIB-type basalt and leucogranite, as respective mixing components, indicates that the involvement of approximately 5–15% OIB-type basalts can explain the isotopic characteristics of the Comei granite (Fig. 7a). A simple mass balance calculation of two end-members also yields similar major element compositions (e.g., SiO_2 and MgO; Supplementary Table A3) to the Comei granite samples, further supporting crust-mantle interaction. In addition, zircon saturation temperatures (T_{Zr}) of the Comei A-type granite samples, calculated using the method proposed by Watson and Harrison (1983) yield 856 ˚C to 910 ˚C (Table 1), which supports a high melting temperature and makes it almost certain that basaltic magmas were involved in their origin, both physically and chemically.

5.1.3 Petrogenesis of the Comei A-type granites

The Early Cretaceous Comei porphyritic granite has major element characteristics of A-type granites including lower CaO contents and higher Zr+Nb+Ce+Y and

FeO^T/MgO and $(Na_2O + K_2O)/Al_2O_3$ ratios compared to calc-alkaline granitoids (e.g., Collins et al., 1982; Whalen et al., 1987; Eby, 1990; Kerr and Fryer, 1993) and metapelite-derived leucogranite (Guo and Wilson, 2012). Thus, a hybrid source, as discussed above, cannot be solely responsible for all these compositional characteristics of the Comei granite, particularly their A-type granite affinity. Previous experimental data indicates that shallow dehydration melting of hornblende- and biotite-bearing protoliths (gneiss or metapelites) can explain the composition of metaluminous A-type granites (Patiño Douce and Beard,1995; Patiño Douce, 1997), and this possibility for the peraluminous Comei porphyritic granite is explored below.

Mineral assemblages in the crustal source of felsic rocks can be further constrained by their geochemical characteristics. Given that plagioclase is enriched in Sr, and garnet is depleted in LREEs and enriched in HREEs and Y, the markedly negative Sr (Sr*/Sr = 0.04–0.09) anomalies, and relatively high $(La/Yb)_{CN}$ (12.0–13.7) and low $(Gd/Yb)_{CN}$ (1.9–2.4) ratios of the Comei porphyritic granites, reflect a source containing residual plagioclase but no garnet. Given that garnet could be stable to pressures as low as 5 kbar during fluid-absent melting of metasedimentary rocks (Patiño Douce and Harris, 1998; García-Casco et al., 2003), the Early Cretaceous Comei granite was likely derived by partial melting of a predominantly metapelite source at shallow crust levels of less than 5 kbar.

Based on experimental data, major element compositions (expressed as CIPW-norms) have been shown to have potential constraints on pressure and fluid activity during granite magma genesis (Inger and Harris, 1993). In the ternary haplogranite system of normative quartz, albite and orthoclase, most of the Comei granite samples plot in region of low pressure (< 2 kbar) and water activity ($a_{H2O}<0.3$)

(Fig.12). If the initial melting reaction is fluid absent, K-feldspar will be generated as a restite phase. Subsequent higher-temperature melting will incorporate this K-feldspar into the melt, causing a shift to more potassic compositions (Inger and Harris, 1993). In addition, potassic Comei granite samples may also result from dehydration melting of micas (as opposed to fluid-saturated melting), consistent with their mica-rich metapelite source (Patiño Douce and Johnston, 1991; Inger and Harris, 1993).

The composition of the Comei granite is also consistent with the modelling reaction curves of melt compositions produced by hybridisation of mantle-derived magmas with minor metasediment-derived melts at low pressure (< 5 kbar) (Fig. 11, Patiño Douce, 1999). Dehydration melting experiments indicate significant amounts of calcic plagioclase and orthopyroxene would form a residual assemblage during low pressure (< 5 kbar) melting. Such a residual assemblage would result in low Ca, Mg, Sr, and Eu contents, and high Ga/Al and K/Na ratios in metaluminous A-type melts (Patiño Douce and Beard, 1995; Patiño Douce, 1997, 1999). However, unlike experimental calc-alkali melts, the Comei granite was derived from a hybrid source mainly composed of metapelites with minor (5–15%) basaltic melts. Metapelitic rocks rich in mica and aluminosilicate and low in plagioclase contain an excess of refractory minerals, thus metapelites are not conducive to the formation of a large volume of magma (Patiño Douce and Johnston, 1991). In addition, a hybrid source of the Comei granite, mainly composed of metapelites, would contain small amounts of calcic plagioclase and orthopyroxene in the residual assemblage leading to relatively low Fe, Mg and Ca contents in the magma. Conversely, the Comei metapelite-derived aluminous A-type granite melts would inherit more K and Al from their source to further distinguish them from typical metaluminous A-type melts.

20

The Comei granite samples have negative Ba, Sr, Nb and Ti anomalies on primitive mantle-normalised trace element plots (Fig. 5) and these patterns are consistent with the presence of residual plagioclase, K-feldspar and biotite in the source region. Additionally, the moderately negative Eu anomalies of the Comei granite samples are similar to the metasediment-derived leucogranites (e.g., Guo and Wilson, 2012) and Higher Himalayan metasediments (Inger and Harris, 1993) (Fig. 5a) and also indicate the presence of residual plagioclase in their source rather than reflecting fractional crystallisation of plagioclase and alkali feldspar. Moreover, the Comei granite also has enriched Th and U and depleted Nb, Ta and Ti contents, which could have been inherited from its metapelite source which is represented by the Lhozhag leucogranites (Fig. 5b).

Despite this evidence, the Comei granite samples have markedly higher REE contents relative to the Lhozhag leucogranites that are also derived from metapelite in Tethyan Himalaya (Guo and Wilson, 2012) (Fig. 5a). Generally, REE patterns in granites are controlled by accessory minerals with high partition coefficients, such as apatite, titanite, zircon, allanite and monazite. The relatively constant chondrite-normalised La/Y ratios (Fig. 5a) in the Comei granite samples suggest the involvement of zircon, apatite and titanite, which all have high and nearly uniform partition coefficients for all REEs (Arth, 1976; Hanson, 1978) and would result in higher overall REE abundances without changing the concavity of REE patterns (Fig. 5a). In contrast, allanite and monazite, that would enhance the skewedness of the concavity toward HREE, were unlikely to have been involved in generation of the Comei granite. Likewise, the negative Zr anomalies of the Lhozhag leucogranites in primitive mantle-normalised trace element patterns (Fig. 5b) imply the presence of residual zircon in their source region, which is supported by abundant ancient zircons

21

in the Higher Himalaya Series (Guo and Wilson, 2012). In contrast, positive Zr anomalies ($Zr/Zr* = 2Zr_{PM}/(Sm_{PM}+P_{PM}) = 1.3–2.6$) of the Comei granite samples, that are derived from a similar source, more likely result from melting of these zircons at higher temperatures. The higher zircon saturation temperatures (856–910 ˚C) of the Comei A-type granite compared to the temperatures (640–740 ˚C) of Himalaya leucogranites (Guo and Wilson, 2012) would facilitate the dissolution in the melt of refractory zircon, apatite and titanite. Sample 11SR17-1 with the highest calculated temperature of 1004 ˚C has the highest REE contents (Table 1) (Fig. 5), which also further confirms this inference.

In summary, the peraluminous Comei A-type granite was emplaced in the Early Cretaceous (ca. 140 Ma) and was produced by interaction between high-temperature upwelling OIB type basaltic magmas and a metapelite source at shallow crustal levels (<16 km). The composition of peraluminous Comei A-type granite was controlled by source components and melting conditions, in particular high temperature and low pressure.

5.2 Tectonic implications

The Early Cretaceous Comei LIP covers an area of ~50000 km^2 in the eastern Tethyan Himalaya of southeastern Tibet and was first proposed to be a LIP by Zhu et al. (2009) (Fig. 1b). U-Pb zircon ages initially indicated that the magmatism occurred between 136–130 Ma with peak age of ca. 132 Ma, coeval with the Bunbury basalts in southwestern Australia (Zhu et al., 2005, 2008, 2009, 2013). However, more-recent geochronological data for the Comei LIP including dates from picrites, basalts and granites yield a wider age range from 145 Ma to 125 Ma (Zhu et al., 2008; Xia et al., 2014; Lv et al., 2016, and this study). U–Pb zircon ages of the Wölong volcaniclastics

in the Tethyan Himalaya also confirm that this volcanism continued from 140 Ma to

119 Ma (Hu et al., 2010). In addition, U–Pb ages of Early Cretaceous detrital zircons

from Cretaceous to the Paleocene sandstones in the region cluster mainly between 142

Ma and 116 Ma in the Tethyan Himalaya (Hu et al., 2015), further indicating the

occurrence of an Early Cretaceous (ca. 145 Ma to 125 Ma) large igneous event in the

eastern Tethyan Himalaya (Fig. 1b).

Various models for tectonic setting and dynamic evolution of the Early Cretaceous

Comei LIP have been proposed, which can be summarised into two basic intra-plate

models: 1) the Comei LIP was linked to the Kerguelen mantle plume, which may have

played a role in the breakup of eastern Gondwana (Zhu et al., 2005, 2007, 2008, 2009,

2013; Hu et al., 2015; Xia et al., 2014); 2) the LIP event resulted from decompression

melting of upwelling mantle caused by intra-continental lithospheric thinning during

extension of Neo-Tethyan passive continental margin (e.g., Zhong et al., 2005; Jiang

et al., 2006, 2007) or breakup of eastern Gondwana (Hu et al., 2010). Detrital spinels

in the Early Cretaceous basalts have an OIB-like composition (Hu et al., 2010) and

coeval magmatic rocks lack arc and back-arc geochemical characteristics (such as

depleted Nb-Ta and relatively low LREE) (Zhu et al., 2008). Both these features

support Early Cretaceous intra-plate magmatism. In addition, the middle Early

Jurassic to the earliest Cretaceous shallow water carbonate-platform sedimentation in

the Tethyan Himalaya indicates a mature passive continental margin setting (Garzanti,

1999; Sciunnach and Garzanti, 2012).

The 145–140 Ma OIB type basalts and A-type granites may represent an earlier

bimodal magmatic event in the eastern Tethyan Himalaya (Zhu et al., 2008 and this

study). Given the occurrence of high temperature (up to 1570 ˚C) picritic rocks and

the large area over which the mafic rocks occur (likely more than 50000 km^2), the later stage (136–125 Ma) magmatism of the LIP in eastern Tethyan Himalaya were proposed to have been the result of melting of a mantle plume (Zhu et al., 2005, 2007, 2009, 2013; Xia et al., 2014). However, the tectono-magmatic settings of the newly identified early stage (145–140 Ma) magmatism are less clear.

Magmatic bimodality, also known as the Bunsen–Daly Gap (Bunsen, 1851; Daly, 1925), is recognised in a variety of tectonic settings and various potential explanations have been proposed (Meade et al., 2014). Previous studies support the derivation of felsic magmas by crustal melting during the emplacement of basalt (e.g., Patchett, 1980; Annen et al., 2006). Large igneous provinces (LIPs) frequently include a significant component of silicic rocks, often in a bimodal (mafic–felsic) series (Bryan et al., 2002). The North Atlantic Igneous Province (NAIP) is one such LIP and formed in response to the opening of the North Atlantic Ocean (62–54 Ma) (Saunders et al., 2007). The associated pre-breakup bimodal continental magmatism includes the British Tertiary Igneous Province (BTIP) (62–56 Ma), where mantle-derived magmas traversed relatively thick, fusible continental crust (e.g., Kerr et al., 1999; Meade et al., 2014 and references therein).

In this study, we propose a similar geodynamic model to explain origin of the earliest Cretaceous Comei bimodal continental magmatism in the eastern Tethyan Himalaya. The earliest Cretaceous bimodal magmatism was at least 10 to 15 Myr earlier than Kerguelen plume magmatism and break-up of eastern Gondwana (Powell et al., 1988; Coffin et al., 2002; Duncan et al., 2002; Kieffer et al., 2002; Ingle et al., 2002; Müller, 2007). The high temperature (~900 ˚C) and A-type affinity of the Comei granite requires a high temperature shallow crustal source. High temperature

mantle-derived OIB type basalts upwelled through crust and triggered partial melting of metapelites that mixed with minor basaltic melts at shallow crustal levels (<16 km).

Lithospheric thickness is considered as an important physical control on the composition of asthenosphere-derived melts by restricting the minimum depth of decompression melting (e.g., Kerr, 1994; Mantle and Collins, 2008; Niu and O'Hara, 2008; Niu et al., 2011). Based on high Ce/Y (up to 2.3) and moderate $(Sm/Yb)_{CN}$ (3.2–5.0) for the 145 Ma OIB type basalts in the eastern Tethyan Himalaya (Zhu et al., 2008), their initial melting was predominantly in the spinel-garnet transition zone (~60–80 km) overlying typical continental crust (~30–35 km). This evidence is strongly suggestive of decompression melting triggered by lithospheric thinning, although the mechanism involved in thinning of the continental lithosphere remains unclear. A high stretching factor (up to 3) and the presence of continental flood basalts suggest a successful rift in the Tethyan Himalaya leading to continental break-up between northern Gondwana and peri-Gondwanian blocks and incipient sea-floor spreading of Neo-Tethyan Early Permian (Garzanti et al., 1999; Sciunnach and Garzanti, 2012).

Subsequently, Tethyan Himalaya (or north margin of Greater India) underwent extension from the Late Triassic and gradually transformed into a stable passive continental margin by the mid-latest Jurassic (e.g., Dai et al., 2008; Garzanti, 1999; Sciunnach and Garzanti, 2012). In the earliest Cretaceous (~145–140 Ma), a rifting event prior to breakup of eastern Gondwana resulted in lithospheric thinning and generation of high-Ti OIB-type basalts and A-type granites in the eastern Tethyan Himalaya (Zhu et al., 2007, 2008 and this study). The Indian continent began to

separate from Australia and Antarctica in Early Cretaceous (ca. 132–130 Ma) (Powell et al., 1988; Patzelt et al., 1996; Li and Powell, 2001; Kumar et al., 2007), then drifted rapidly northward and collided with Asian continent (Yin and Harrison, 2000). The ca.132–123 Ma Bunbury basalt of western Australia (e.g., Frey et al., 1996) and the ca. 120–110 Ma bimodal volcanism of the Kerguelen Plateau (Duncan et al., 2002; Kieffer et al., 2002) were then triggered by the Kerguelen Plume (Ingle et al., 2002), which also resulted in the opening of the eastern Indian Ocean at 130.9 Ma (e.g., Heine and Müller, 2005; Müller, 2007).

In summary, the earliest Cretaceous OIB type basalt formed by decompression melting. This melt rose through the crust and interacted with shallow crustal metapelites resulting in bimodal continental magmatism during pre-breakup lithospheric thinning.

6. Conclusions

1. The Comei porphyritic granite was emplaced in the Early Cretaceous (ca. 140 Ma) and is characterised by peraluminous A-type granite affinities with high SiO_2 and Ga/Al ratios and low CaO and Na_2O contents along high FeO^{total}/MgO, $(Na_2O + K_2O)/Al_2O_3$ and A/CNK (1.00–1.36) ratios.

2. The Comei granite was derived from a hybrid source and formed by interaction between high-temperature upwelling OIB-type basaltic magmas and a metapelite source at shallow (<16 km) crustal levels.

3. The composition of peraluminous Comei A-type granite was controlled by source components together with melting conditions, in particular high temperature and low pressure.

4. The earliest Cretaceous (ca. 140 Ma) Comei granite and coeval OIB type basaltic rocks could represent an earlier bimodal magmatic event in the eastern Tethyan Himalaya, which was trigged by pre-breakup lithospheric thinning prior to the arrival of the Kerguelen plume head.

REFERENCES

Altherr, R., Siebel, W., 2002. I-type plutonism in a continental back-arc setting: Miocene granitoids and monzonites from the central Aegean Sea, Greece. Contributions to Mineralogy and Petrology 143, 397-415

Altherr, R., Holl, A., Hegner, E., Langer, C., Kreuzer, H., 2000. High-potassium, calc-alkaline I-type plutonism in the European Variscides: northern Vosges (France) and northern Schwarzwald (Germany). Lithos 50, 51-73.

Annen, C., Blundy, J., Sparks, R., 2006. The genesis of intermediate and silicic magmas in deep crustal hot zones. Journal of Petrology 47, 505-539.

Arculus, R.J., 2003. Use and abuse of the terms calcalkaline and calcalkalic. Journal of Petrology 44, 929-935.

Arth, J.G., 1976. Behavior of trace elements during magmatic processes: a summary of theoretical models and their applications. J. Res. US Geol. Surv. 4(1), 41-47.

Bédard, J., 1990. Enclaves from the A-type granite of the Megantic Complex, White Mountain Magma Series: Clues to granite magmagenesis. Journal of Geophysical Research 95, 17797-17819.

Bienvenu, P., Bougault, H., Joron, J., Treuil, M., Dmitriev, L., 1990. MORB alteration: rare-earth element/non-rare-earth hygromagmaphile element fractionation. Chemical Geology 82, 1-14.

Black, L.P., Kamo, S.L., Allen, C.M., Aleinikoff, J.N., Davis, D.W., Korsch, R.J., Foudoulis, C., 2003. TEMORA 1: a new zircon standard for Phanerozoic U-Pb geochronology. Chemical Geology 200, 155-170.

Bryan, S.E., Riley, T.R., Jerram, D.A., Stephens, C.J., Leat, P.T., 2002. Silicic volcanism: an undervalued component of large igneous provinces and volcanic rifted margins. Special Papers-Geological Society of America, 97-118.

Bunsen, R., 1851. Ueber die Processe der vulkanischen Gesteinsbildungen Islands. Annalen der Physik 159, 197-272.

Clemens, J.D., Holloway, J.R., White, A.J.R., 1986. Origin of an A-type granite: experimental constraints. American Mineralogist 71, 317-324.

Coffin, M.F., Pringle, M., Duncan, R., Gladczenko, T., Storey, M., Müller, R., Gahagan, L., 2002. Kerguelen hotspot magma output since 130 Ma. Journal of Petrology 43, 1121-1137.

Coleman, M.E., 1998. U-Pb constraints on Oligocene-Miocene deformation and anatexis within the central Himalaya, Marsyandi Valley, Nepal. American Journal of Science 298, 553-571.

Collins, W., Beams, S., White, A., Chappell, B., 1982. Nature and origin of A-type granites with particular reference to southeastern Australia. Contributions to mineralogy and petrology 80, 189-200.

Dai, J., Yin, A., Liu, W., Wang, C., 2008. Nd isotopic compositions of the Tethyan Himalayan Sequence in southeastern Tibet. Science in China Series D: Earth Sciences 51, 1306-1316.

Daly, R.A., 1925. The geology of ascension island, Proceedings of the American Academy of Arts and Sciences 60(1), 3-80.

Ding, L., Kapp, P., Wan, X., 2005. Paleocene–Eocene record of ophiolite obduction and initial India‐Asia collision, south central Tibet. Tectonics 24, TC3001, doi:10.1029/2004TC001729.

Duncan, R.A., 2002. A time frame for construction of the Kerguelen Plateau and Broken Ridge. Journal of Petrology 43, 1109-1119.

Eby, G.N., 1990. The A-type granitoids: a review of their occurrence and chemical characteristics and speculations on their petrogenesis. Lithos 26, 115-134.

Eby, G.N., 1992. Chemical subdivision of the A-type granitoids: petrogenetic and tectonic implications. Geology 20, 641-644.

Faure, G., 1986. Principles of isotope geology. John Wiley & Sons, New York.

Frey, F.A., McNaughton, N.J., Nelson, D.R., Duncan, R.A., 1996. Petrogenesis of the Bunbury Basalt, Western Australia: interaction between the Kerguelen plume and Gondwana lithosphere? Earth and Planetary Science Letters 144, 163-183.

García-Casco, A., Haissen, F., Castro, A., El-Hmidi, H., Torres-Roldán, R.L., Millán, G., 2003. Synthesis of Staurolite in Melting Experiments of a Natural Metapelite: Consequences for the Phase Relations in Low-Temperature Pelitic Migmatites. Journal of Petrology 44, 1727-1757.

Garzanti, E., 1999. Stratigraphy and sedimentary history of the Nepal Tethys Himalaya passive margin. Journal of Asian Earth Sciences 17, 805-827.

Garzanti, E., Le Fort, P., Sciunnach, D., 1999. First report of Lower Permian basalts in South Tibet: tholeiitic magmatism during break-up and incipient opening of Neotethys. Journal of Asian Earth Sciences 17, 533-546.

Gelman, S.E., Deering, C.D., Bachmann, O., Huber, C., Gutiérrez, F.J., 2014. Identifying the crystal graveyards remaining after large silicic eruptions. Earth and Planetary Science Letters 403, 299-306.

Guo, Z., Wilson, M., 2012. The Himalayan leucogranites: constraints on the nature of their crustal source region and geodynamic setting. Gondwana Research 22, 360-376.

Hanson, G.N., 1978. The application of trace elements to the petrogenesis of igneous rocks of granitic composition. Earth and Planetary Science Letters 38, 26-43.

Harris, N.B.W., Gravestock, P., Inger, S., 1992. Ion-microprobe determinations of trace-element concentrations in garnets from anatectic assemblages. Chemical Geology 100, 41-49.

Harrison, M.T., Grove, M., Mckeegan, K.D., Coath, C., Lovera, O.M., Le Fort, P., 1999. Origin and episodic emplacement of the Manaslu intrusive complex, central Himalaya. Journal of Petrology 40, 3-19.

Hawkesworth, C., Turner, S., McDermott, F., Peate, D., Van Calsteren, P., 1997. U-Th isotopes in arc magmas: Implications for element transfer from the subducted crust. Science 276, 551-555.

Heine, C., Müller, R., 2005. Late Jurassic rifting along the Australian North West Shelf: margin geometry and spreading ridge configuration. Australian Journal of Earth Sciences 52, 27-39.

Hoskin, P., Black, L., 2000. Metamorphic zircon formation by solid state recrystallization of protolith igneous zircon. Journal of metamorphic Geology 18, 423-439.

Hou, Z.-Q., Zheng, Y.-C., Zeng, L.-S., Gao, L.-E., Huang, K.-X., Li, W., Li, Q.-Y., Fu, Q., Liang, W., Sun, Q.-Z., 2012. Eocene–Oligocene granitoids in southern Tibet: constraints on crustal anatexis and tectonic evolution of the Himalayan orogen. Earth and Planetary Science Letters 349, 38-52.

Hu, X.-M., Garzanti, E., An, W., Hu, X.-F., 2015. Provenance and drainage system of the Early Cretaceous volcanic detritus in the Himalaya as constrained by detrital zircon geochronology. Journal of Palaeogeography 4, 85-98.

Hu, X., Jansa, L., Chen, L., Griffin, W.L., O'Reilly, S.Y., Wang, J., 2010. Provenance of Lower Cretaceous Wölong volcaniclastics in the Tibetan Tethyan Himalaya: Implications for the final breakup of eastern Gondwana. Sedimentary Geology 223, 193-205.

Huang, H.-Q., Li, X.-H., Li, W.-X., Li, Z.-X., 2011. Formation of high $\delta^{18}O$ fayalite-bearing A-type granite by high-temperature melting of granulitic metasedimentary rocks, southern China. Geology 39, 903-906.

Huang, X.L., Xu, Y.G., Lo, C.H., Wang, R.C., Lin, C.Y., 2007. Exsolution lamellae in a clinopyroxene megacryst aggregate from Cenozoic basalt, Leizhou Peninsula, South China: petrography and chemical evolution. Contributions to Mineralogy and Petrology 154, 691-705.

Inger, S., Harris, N., 1993. Geochemical constraints on leucogranite magmatism in the Langtang Valley, Nepal Himalaya. Journal of Petrology 34, 345-368.

Ingle, S., Weis, D., Scoates, J.S., Frey, F.A., 2002. Relationship between the early Kerguelen plume and continental flood basalts of the paleo-Eastern Gondwanan margins. Earth and Planetary Science Letters 197, 35-50.

Jiang, S., Nie, F., Peng, H.U., Liu, Y., 2006. An Important Spreading Event of the Neo-Tethys Ocean during the Late Jurassic and Early Cretaceous: Evidence from Zircon U-Pb SHRIMP Dating on Diabase in Nagarze, Southern Tibet. Acta Geologica Sinica 80, 522-527.

Jiang, S., Nie, F., Hu, P., Liu, Y., Lai, X., 2007. Geochemical characteristics of the mafic dykes warms in South Tibet. Acta Geologica Sinica 81, 60-71.

Jweda, J., Bolge, L., Class, C., Goldstein, S.L., 2016. High Precision Sr-Nd-Hf-Pb Isotopic Compositions of USGS Reference Material BCR-2. Geostandards and Geoanalytical Research 40, 101-115.

Kerr, A., Fryer, B.J., 1993. Nd isotope evidence for crust-mantle interaction in the generation of A-type granitoid suites in Labrador, Canada. Chemical Geology 104, 39-60.

Kerr, A.C., 1994. Lithospheric thinning during the evolution of continental large igneous provinces: A case study from the North Atlantic Tertiary province. Geology 22, 1027-1030.

Kerr, A.C., Kent, R.W., Thomson, B.A., Seedhouse, J.K., Donaldson, C.H., 1999. Geochemical evolution of the Tertiary Mull volcano, western Scotland. Journal of Petrology 40, 873-908.

Kieffer, B., Arndt, N.T., Weis, D., 2002. A bimodal alkalic shield volcano on Skiff Bank: Its place in the evolution of the Kerguelen Plateau. Journal of Petrology 43, 1259-1286.

King, J., Harris, N., Argles, T., Parrish, R., Zhang, H., 2011. Contribution of crustal anatexis to the tectonic evolution of Indian crust beneath southern Tibet. Geological Society of America Bulletin 123, 218-239.

King, P., Chappell, B., Allen, C.M., White, A., 2001. Are A-type granites the high‐temperature felsic granites? Evidence from fractionated granites of the Wangrah Suite. Australian Journal of Earth Sciences 48, 501-514.

King, P., White, A., Chappell, B., Allen, C., 1997. Characterization and origin of aluminous A-type granites from the Lachlan Fold Belt, southeastern Australia. Journal of Petrology 38, 371-391.

Kumar, P., Yuan, X., Kumar, M.R., Kind, R., Li, X., Chadha, R., 2007. The rapid drift of the Indian tectonic plate. Nature 449, 894-897.

Lee, C.T.A., Morton, D.M., 2015. High silica granites: Terminal porosity and crystal settling in shallow magma chambers. Earth and Planetary Science Letters 409, 23-31.

Le Fort, P., Cuney, M., Deniel, C., France-Lanord, C., Sheppard, S., Upreti, B., Vidal, P., 1987. Crustal generation of the Himalayan leucogranites. Tectonophysics 134, 39-57.

Li, Z., Powell, C.M., 2001. An outline of the palaeogeographic evolution of the Australasian region since the beginning of the Neoproterozoic. Earth-Science Reviews 53, 237-277.

Li, X.-H., Li, W.-X., Li, Q.-L., Wang, X.-C., Liu, Y., Yang, Y.-H., 2010. Petrogenesis and tectonic significance of the~ 850 Ma Gangbian alkaline complex in South China: evidence from in situ zircon U–Pb dating, Hf–O isotopes and whole-rock geochemistry. Lithos 114, 1-15.

Li, X., Tang, G., Gong, B., Yang, Y., Hou, K., Hu, Z., Li, Q., Liu, Y., Li, W., 2013. Qinghu zircon: A working reference for microbeam analysis of U-Pb age and Hf and O isotopes. Chinese Science Bulletin 58, 4647-4654.

Li, X.H., Liu, D., Sun, M., Li, W.X., Liang, X.R., Liu, Y., 2004. Precise Sm-Nd and U-Pb isotopic dating of the supergiant Shizhuyuan polymetallic deposit and its host granite, SE China. Geological Magazine 141(2), 225-231.

Li, X.H., Qi, C.S., Liu, Y., Liang, X.R., Tu, X.L., Xie, L.W., Yang, Y.H., 2005. Petrogenesis of the Neoproterozoic bimodal volcanic rocks along the western margin of the Yangtze Block: new constraints from Hf isotopes and Fe/Mn ratios. Chinese Science Bulletin 50, 2481-2486.

Liu, Z.C., Wu, F.Y., Ji, W.Q., Wang, J.G., Liu, C.Z., 2014. Petrogenesis of the Ramba leucogranite in the Tethyan Himalaya and constraints on the channel flow model. Lithos 208, 118-136.

Liu, Z.C., Wu, F.Y., Ding, L., Liu, X.C., Wang, J.G., Ji, W.Q., 2016. Highly fractionated Late Eocene (~ 35Ma) leucogranite in the Xiaru Dome, Tethyan Himalaya, South Tibet. Lithos 240, 337-354.

Lizumi, S., Morris, P. A., Sawada, Y., 1995. Nd isotope data for GSJ reference samples JB-la, JB-3 and JG-1 a and the La Jolla standard. Mem. Fac. Sci. Shimane Univ. 29, 73-76.

Loiselle, M., Wones, D., 1979. Characteristics and origin of anorogenic granites, Geological Society of America Abstracts with Programs, 11, 468.

Ludwig, K. R., 2003. ISOPLOT 3.00: A Geochronological Toolkit for Microsoft Excel. Berkeley: Berkeley Geochronology Center, California.

Lv, X., Ren, C., Wu, R., Cheng, M., Qiu, H., Qiu, Y., 2016. Discovery of bimodal volcanics in Longzi area, Southern Xizang: evidence from SHRIMP U-Pb zircon age and geochemical analysis. Geological Review 62, 945-954.

Mahoney, J.J., Frei, R., Tejada, M., Mo, X., Leat, P., Nägler, T., 1998. Tracing the Indian Ocean mantle domain through time: isotopic results from old West Indian, East Tethyan, and South Pacific seafloor. Journal of Petrology 39, 1285-1306.

Maniar, P.D., Piccoli, P.M., 1989. Tectonic discrimination of granitoids. Geological society of America bulletin 101, 635-643.

Mantle, G., Collins, W., 2008. Quantifying crustal thickness variations in evolving orogens: Correlation between arc basalt composition and Moho depth. Geology 36, 87-90.

Mcdermott, F., Hawkesworth, C., 1990. The evolution of strontium isotopes in the upper continental crust. Nature 344, 850-853.

Meade, F., Troll, V., Ellam, R., Freda, C., Font, L., Donaldson, C., Klonowska, I., 2014. Bimodal magmatism produced by progressively inhibited crustal assimilation. Nature Communications 5:4199, DOI: 10.1038/ncomms5199.

Middlemost, E.A., 1994. Naming materials in the magma/igneous rock system. Earth-Science Reviews 37, 215-224.

Miyashiro, A., 1974. Volcanic rock series in island arcs and active continental margins. American Journal of Science 274, 321-355.

Müller, R.D., 2007. Earth science: An Indian cheetah. Nature 449, 795-796.

Niu, Y., O'Hara, M.J., 2008. Global correlations of ocean ridge basalt chemistry with axial depth: a new perspective. Journal of Petrology 49, 633-664.

Niu, Y., Wilson, M., Humphreys, E.R., O'Hara, M.J., 2011. The origin of intra-plate ocean island basalts (OIB): the lid effect and its geodynamic implications. Journal of Petrology 52, 1443-1468.

Okano, O., Kanazawa, R., Tosa, H., Matsumoto, H., 1989. Sr, Nd and Ce isotopic measurements of GSJ standard rocks using MAT 262 equipped with variable multicollector system. Abstract 1989 Nihon Chikyu-Kagakukai Nenkai, 268 (in Japanese).

Patchett, P., 1980. Thermal effects of basalt on continental crust and crustal contamination of magmas. Nature 283, 559-561.

Patiño Douce, A.E., Beard, J.S., 1995. Dehydration-melting of biotite gneiss and quartz amphibolite from 3 to 15 kbar. Journal of Petrology 36, 707-738.

Patiño Douce, A.E., Johnston, A.D., 1991. Phase equilibria and melt productivity in the pelitic system: implications for the origin of peraluminous granitoids and aluminous granulites. Contributions to Mineralogy and Petrology 107, 202-218.

Patiño Douce, A.E., 1997. Generation of metaluminous A-type granites by low-pressure melting of calc-alkaline granitoids. Geology 25, 743-746.

Patiño Douce, A.E., 1999. What do experiments tell us about the relative contributions of crust and mantle to the origin of granitic magmas? Geological Society, London, Special Publication 168, 55-75.

Patiño Douce, A.E., Harris, N., 1998. Experimental Constraints on Himalayan Anatexis. Journal of Petrology 39, 689-710.

Patzelt, A., Li, H., Wang, J., Appel, E., 1996. Palaeomagnetism of Cretaceous to Tertiary sediments from southern Tibet: evidence for the extent of the northern margin of India prior to the collision with Eurasia. Tectonophysics 259, 259-284.

Pearce, N.J., Perkins, W.T., Westgate, J.A., Gorton, M.P., Jackson, S.E., Neal, C.R., Chenery, S.P., 1997. A compilation of new and published major and trace element data for NIST SRM 610 and NIST SRM 612 glass reference materials. Geostandards and Geoanalytical Research 21, 115-144.

Pearce, J.A., Harris, N.B., Tindle, A.G., 1984. Trace element discrimination diagrams for the tectonic interpretation of granitic rocks. Journal of Petrology 25, 956-983.

Peccerillo, A., Taylor, S.R., 1976. Geochemistry of Eocene calc-alkaline volcanic rocks from the Kastamonu area, northern Turkey. Contributions to Mineralogy and Petrology 58, 63-81.

Peck, W.H., Valley, J.W., Graham, C.M., 2003. Slow oxygen diffusion rates in igneous zircons from metamorphic rocks: American Mineralogist 88, 1003–1014.

Powell, C.M., Roots, S., Veevers, J., 1988. Pre-breakup continental extension in East Gondwanaland and the early opening of the eastern Indian Ocean. Tectonophysics 155, 261-283.

Richards, A., Argles, T., Harris, N., Parrish, R., Ahmad, T., Darbyshire, F., Draganits, E., 2005. Himalayan architecture constrained by isotopic tracers from clastic sediments. Earth and Planetary Science Letters 236, 773-796.

Saunders, A., Jones, S., Morgan, L., Pierce, K., Widdowson, M., Xu, Y., 2007. Regional uplift associated with continental large igneous provinces: the roles of mantle plumes and the lithosphere. Chemical Geology 241, 282-318.

Sciunnach, D., Garzanti, E., 2012. Subsidence history of the Tethys Himalaya. Earth-Science Reviews 111, 179-198.

Skjerlie, K.P., Johnston, A.D., 1993. Fluid-Absent Melting Behavior of an F-Rich Tonalitic Gneiss at Mid-Crustal Pressures: Implications for the Generation of Anorogenic Granites. Journal of Petrology 34, 785-815.

Sláma, J., Košler, J., Condon, D.J., Crowley, J.L., Gerdes, A., Hanchar, J.M., Horstwood, M.S., Morris, G.A., Nasdala, L., Norberg, N., 2008. Plešovice zircon—a new natural reference material for U–Pb and Hf isotopic microanalysis. Chemical Geology 249, 1-35.

Staudigel, H., Plank, T., White, B., Schmincke, H.U., 1996. Geochemical fluxes during seafloor alteration of the basaltic upper oceanic crust: DSDP Sites 417 and 418. Geophysical monograph 96, 19-38.

Sun, S.S., McDonough, W., 1989. Chemical and isotopic systematics of oceanic basalts: implications for mantle composition and processes. Geological Society, London, Special Publications 42, 313-345.

Taylor, S.R., McLennan, S.M., 1985. The continental crust: its composition and evolution. Blackwell Scientific Pub., Palo Alto, CA.

Turner, S., Foden, J., Morrison, R., 1992. Derivation of some A-type magmas by fractionation of basaltic magma: an example from the Padthaway Ridge, South Australia. Lithos 28, 151-179.

Turner, S., Hawkesworth, C., 1997. Constraints on flux rates and mantle dynamics beneath island arcs from Tonga-Kermadec lava geochemistry. Nature 389, 568-573.

Valley, J., Lackey, J., Cavosie, A., Clechenko, C., Spicuzza, M., Basei, M., Bindeman, I., Ferreira, V., Sial, A., King, E., 2005. 4.4 billion years of crustal maturation: oxygen isotope ratios of magmatic zircon. Contributions to Mineralogy and Petrology 150, 561-580.

Wang Q., Wyman D.A., Li Z.X., Bao Z.W., Zhao Z.H., Wang Y.X., Jian P., Yang Y.H., Chen L.L., 2010. Petrology, geochronology and geochemistry of ca. 780 Ma A-type granites in South China: Petrogenesis and implications for crustal growth during the breakup of supercontinent Rodinia. Precambrian Research 178, 185–208.

Watson, E.B., Harrison, T.M., 1983. Zircon saturation revisited: temperature and composition effects in a variety of crustal magma types. Earth and Planetary Science Letters 64, 295-304.

Wei, G.J., Liang, X.R., Li, X.H., Liu, Y., 2002. Precise measurement of Sr isotopic compositions of liquid and solid base using (LP) MCICP-MS. Geochimica 31, 295-305 (in Chinese with English abstract).

Whalen, J.B., Currie, K.L., Chappell, B.W., 1987. A-type granites: geochemical characteristics, discrimination and petrogenesis. Contributions to Mineralogy and Petrology 95, 407-419.

Wu, F.Y., Sun, D.Y., Li, H., Jahn, B.M., Wilde, S., 2002. A-type granites in northeastern China: age and geochemical constraints on their petrogenesis. Chemical Geology 187, 143-173.

Wu, F., Liu, X., Ji, W., Wang, J., Yang, L., 2017. Highly fractionated granites: Recognition and research. Science China: Earth Sciences 60:7, 1201-1219.

Wu, F.Y., Liu, Z.C., Liu, X.C., Ji, W.Q., 2015. Himalayan leucogranite: pterogenesis and implications to orogenesis and plateau uplift. Acta Petrologica Sinica 31, 1-36.

Xia, Y., Zhu, D.C., Wang, Q., Zhao, Z.D., Liu, D., Wang, L.Q., Mo, X.X., 2014. Picritic porphyrites and associated basalts from the remnant Comei Large Igneous Province in SE Tibet: records of mantle‐plume activity. Terra Nova 26, 487-494.

Yang, J.H., Wu, F.Y., Chung, S.L., Wilde, S.A., Chu, M.F., 2006. A hybrid origin for the Qianshan A-type granite, northeast China: geochemical and Sr–Nd–Hf isotopic evidence. Lithos 89, 89-106.

Yin, A., Harrison, T.M., 2000. Geologic evolution of the Himalayan-Tibetan orogen. Annual Review of Earth and Planetary Sciences 28, 211-280.

Yin, A., 2006. Cenozoic tectonic evolution of the Himalayan orogen as constrained by along-strike variation of structural geometry, exhumation history, and foreland sedimentation. Earth-Science Reviews 76, 1-131.

Zeng, L., Gao, L.-E., Xie, K., Liu-Zeng, J., 2011. Mid-Eocene high Sr/Y granites in the Northern Himalayan Gneiss Domes: melting thickened lower continental crust. Earth and Planetary Science Letters 303, 251-266.

Zhang, H., Harris, N., Parrish, R., Kelley, S., Zhang, L., Rogers, N., Argles, T., King, J., 2004. Causes and consequences of protracted melting of the mid-crust exposed in the North Himalayan antiform. Earth and Planetary Science Letters 228, 195-212.

Zhao, X.F., Zhou, M.F., Li, J.W., Wu, F.Y., 2008. Association of Neoproterozoic A-and I-type granites in South China: implications for generation of A-type granites in a subduction-related environment. Chemical Geology 257, 1-15.

Zhong, H.M., Tong, J.S., Xia, J., Lu, R.K., Qiu, J.Q., 2005. Characteristics and tectonic setting of volcanic rocks of the Sangxiu Formation in the southern part of Yamzho Yumco, southern Tibet. Geological Bulletin of China 24, 72-79.

Zhu, D.C., Chung, S.L., Mo, X.X., Zhao, Z.D., Niu, Y., Song, B., Yang, Y.-H., 2009. The 132 Ma Comei-Bunbury large igneous province: Remnants identified in present-day southeastern Tibet and southwestern Australia. Geology 37, 583-586.

Zhu, D., Mo, X., Pan, G., Zhao, Z., Dong, G., Shi, Y., Liao, Z., Zhou, C., 2008. Petrogenesis of the earliest Early Cretaceous basalts and associated diabases from Cona area, eastern Tethyan Himalaya in south Tibet: interaction between the incubating Kerguelen plume and eastern Greater India lithosphere. Lithos 100, 147-173.

Zhu, D., Pan, G., Mo, X., Liao, Z., Jiang, X., Wang, L., Zhao, Z., 2007. Petrogenesis of volcanic rocks in the Sangxiu Formation, central segment of Tethyan Himalaya: A probable example of plume–lithosphere interaction. Journal of Asian Earth Sciences 29, 320-335.

Zhu, D., Pan, G., Mo, X., Wang, L., Liao, Z., Jiang, X., Geng, Q., 2005. SHRIMP U-Pb zircon dating for the dacite of the Sangxiu Formation in the central segment of Tethyan Himalaya and its implications. Chinese Science Bulletin 50, 563-568.

Zhu, D., Xia, Y., Qiu, B., Wang, Q., Zhao, Z., 2013. Why do we need to propose the Early Cretaceous Comei large igneous province in southeastern Tibet? Acta Petrologica Sinica 29, 3659-3670.

Fig.1. (a) Geological map of the Himalaya Block (modified from Guo and Wilson (2012) and Liu et al. (2014)). Abbreviations: MBT= Main Boundary Thrust; MCT = Main Central Thrust; STDS = South Tibet Detachment System. (b) Detailed occurrences of the Early Cretaceous large igneous province in the eastern Tethyan Himalaya. Yellow boxes mark the locations of zircon U–Pb isotopic ages of the Early Cretaceous magmatic rocks (including published data and from this study) and further details are listed in Supplementary Table A1. (c) A geological map of the Comei area showing the sampling locations in this study.

Fig.2. Petrography of the Comei granite porphyries in the eastern Tethyan Himalaya: (a) miarolitic cavities; (b) plagioclase phenocryst; (c) the quartz phenocryst; (d) widespread occurrence of chlorite; (e) carbonised plagioclase and (f) crystal holes. Abbreviations: Pl–plagioclase; Chl–chlorite; Cal–calcite and Qtz–quartz.

Fig.3. Zircon U–Pb Terra–Wasserburg diagram of the Comei granite samples (a) 11SN19-1 (LA-ICP-MS) and 09TB116-1 (SIMS).

Fig.4. (a) SiO_2 vs. Na_2O+K_2O classification diagram (after Middlemost (1994)); (b) SiO_2 vs. K_2O plot (after Peccerillo and Taylor (1976)); (c) SiO_2 versus FeO^T/MgO diagrams (Miyashiro, 1974), and boundaries (greylines) between low-, medium-, and high-Fe suites are after Arculus (2003); (d) A/NK versus A/CNK diagram (Maniar and Piccoli, 1989). Data sources: Early Cretaceous Tethyan Himalaya (TH) A-type granites (dacites) are from Zhu et al. (2007); Early Cretaceous Tethyan Himalaya (TH) basaltic rocks are from Zhu et al. (2007, 2008); Eocene TH high Sr/Y granites are from Zeng et al. (2011) and Liu et al. (2014); Miocene-Oligocene Himalaya (High Himalaya and Tethyan Himalaya) leucogranites are from Guo and Wilson (2012).

Fig.5. (a) Chondrite-normalised REE and (b) primitive mantle-normalised trace element diagrams of the Comei granite. Data sources: Early Cretaceous Tethyan Himalaya (TH) A-type dacites are from Zhu et al. (2007); Eocene TH high Sr/Y granites are from Zeng et al. (2011); Oligocene Lhozhag leucogranites are from Guo and Wilson (2012). Chondrite and primitive mantle normalization values are from Sun and McDonough (1989).

Fig.6. (a) Na_2O+K_2O, (b) Zr and (c) Nb vs. 10,000 Ga/Al and (d) $(Na_2O+K_2O)/CaO$ vs. (Zr+Nb+Ce+Y) discrimination diagrams of Whalen et al. (1987), showing the A-type nature of the Comei granite. I and S: unfractionated I- and S-type granites; FG: fractionated felsic granites (after Yang et al., 2009).

Fig.7. (a) $\varepsilon_{Nd}(t)$ vs. $(^{87}Sr/^{86}Sr)_t$ and (b) $\varepsilon_{Nd}(t)$ vs. age diagram for the Comei granite samples. Data sources are same as in figure 4. Additional data sources: Yarlung Zangbo ophiolites - Mahoney et al. (1998); Early Cretaceous N-MORB type and OIB type mafic rocks - Zhu et al. (2008); Higher Himalayan (HH) crystalline series and Tethyan Himalaya (TH) sedimentary series are from Richard et al. (2005). The mixing end-members are: TH Early Cretaceous OIB type basalt (CN23-1: $\varepsilon_{Nd}(t)$ = +4.3, $(^{87}Sr/^{86}Sr)_t$ = 0.7037, Nd = 40.7 ppm and Sr = 529 ppm) from Zhu et al. (2008); TH Lhozhag leucogranites (LG-17: $\varepsilon_{Nd}(t)$ = -16.9, $(^{87}Sr/^{86}Sr)_t$ = 0.7323, Nd = 12.8 ppm, Sr = 107 ppm and LG-02: $\varepsilon_{Nd}(t)$ = -16.6, $(^{87}Sr/^{86}Sr)_t$ = 0.7426, Nd = 28.5 ppm, Sr = 146 ppm) from Guo and Wilson (2012).The bivariate mixture calculation use mixing equation of Faure (1986) and indicate a hybrid source consist of metapelite and minor (5-15%) basaltic melt. Reference T_{DM} age evolution for 1.4Ga, 1.7 Ga, 2.0 Ga and 2.5 Ga average continental crust were calculated assuming a typical $^{147}Sm/^{144}Nd$ ratio = 0.12.

Fig.8. (a) Rb, (b) Ba, (c) Sr, (d) Th, (e) U contents and (f) initial $^{87}Sr/^{86}Sr$ ratios vs. loss on ignition (LOI) discrimination diagrams for the Comei granite.

Fig.9. (a) Nb/U vs. Nb and (b) Ce/Y vs. 100Rb/Ba diagrams. The Comei granite has a similar composition to upper continental crust (UCC). Data sources: OIB and N-MORB from Sun and McDonough (1989); UCC and lower continental crust (LCC) from Taylor and McLennan (1985).

Fig.10. (a) molar K_2O/Na_2O, (b) Na_2O, (c) $Mg^{\#}$ and (d) molar $Al_2O_3/(MgO+FeO^T)$ vs. molar

CaO/(MgO+FeO^T) diagrams and showing the composition of the Comei granite (symbols as in Fig. 4), compared to compositional ranges of crustal melts (meta-greywackes, meta-pelites, meta-andesite and meta-basalt after Altherr et al. (2000) and Altherr and Siebel (2002).

Fig.11. Compositions of the Comei granite (symbols as in Fig. 4), compared to compositional ranges of experimental metasediment-derived melts (greywackes, felsic and mafic pelites, after Patiño Douce, 1999). The dash-dot lines and thick solid lines are reaction curves that model compositions of melt produced by hybridization of high-Al olivine tholeiite with metagreywacke at low pressure (LP, P < 5 kbar) and high pressure (HP, P = 12–15 kbar), respectively (Patifio Douce, 1999). Distribution trend indicate that the Comei granite was likely the product of crustal melting at low pressure of less than 5 kbar.

Fig.12. CIPW normative Quartz-Albite-Orthoclase diagram (after Inger and Harris, 1993).

Figure 1

Figure 2

Figure 3

(a)

Mean $^{206}Pb/^{238}U$ age = 139.6±1.8 (2σ)
n=12; MSWD=0.057

11SN19-3

$^{238}U/^{206}Pb$

$^{207}Pb/^{206}Pb$

150 140 130

(b)

Mean $^{206}Pb/^{238}U$ age = 139.7 ± 1.4 (2σ)
n=22; MSWD=1.8

09TB116-1

$^{238}U/^{206}Pb$

$^{207}Pb/^{206}Pb$

156 152 148 144 140 136 132 128

Figure 4

Figure 5

Figure 6

Figure 17

(a)

Yarlung Zangbo Ophiolites

Early Cretaceous
N-MORE type mafic rocks

CN23-1

Early Cretaceous
OIB type mafic rocks

TH high Sr/Y
granites

HH Crystalline Series

Tethyan
Sedimentary Series

LG-17   LG-02

Himalayan Leucogranites

This study
THA-type dacite

$\varepsilon_{Nd}(t)$

$(^{87}Sr/^{86}Sr)_i$

(b)

DM

TH OIB-type basalt
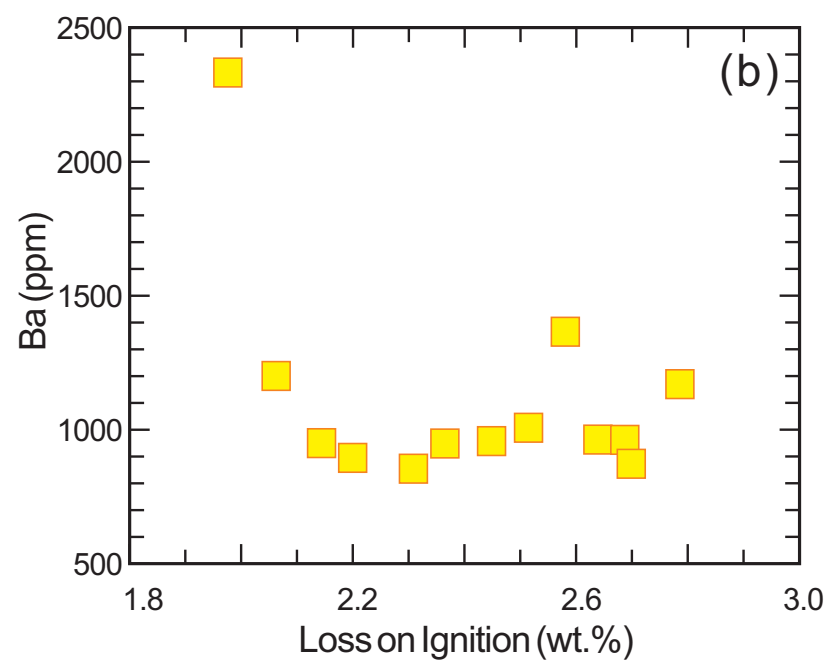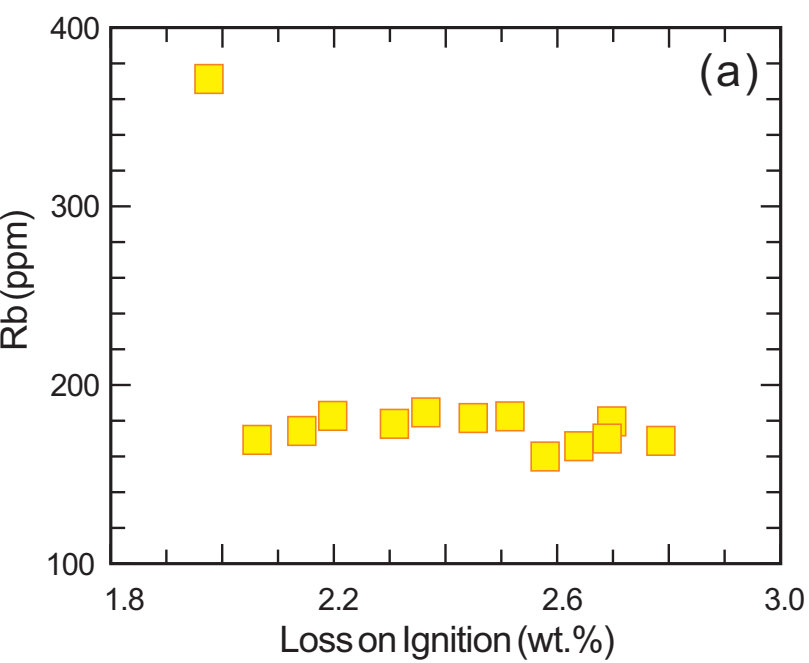Himalaya Leucogranite

CHUR

1.4 Ga

1.7 Ga

2.0 Ga

2.5 Ga

$\varepsilon_{Nd}(t)$

Age (Ma)

Figure 8

Figure 9

Figure 10

Figure 11

Figure 12

Table 1
Click here to download Table: Table 1.docx

Table 1 Major (wt.%) and trace (ppm) elements data for the Comei granite porphyries

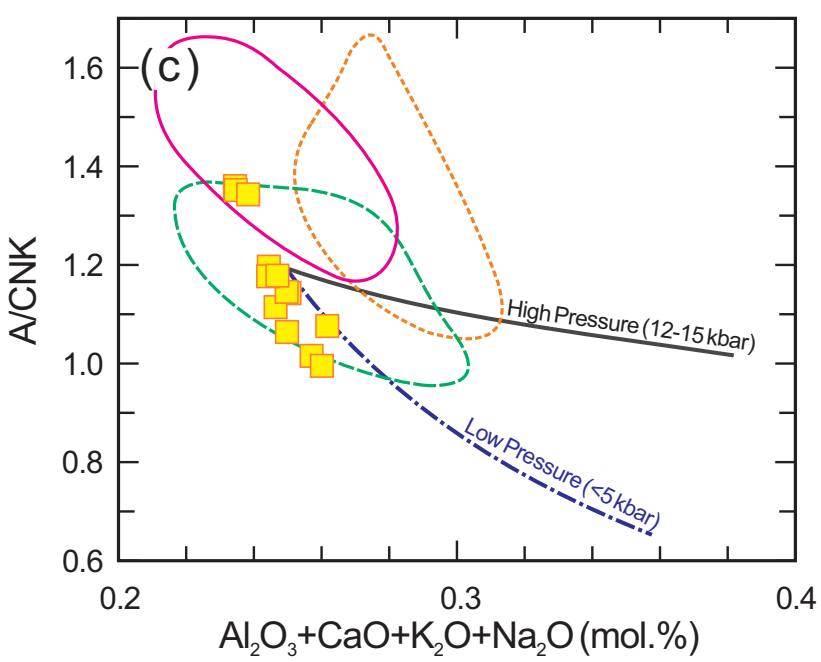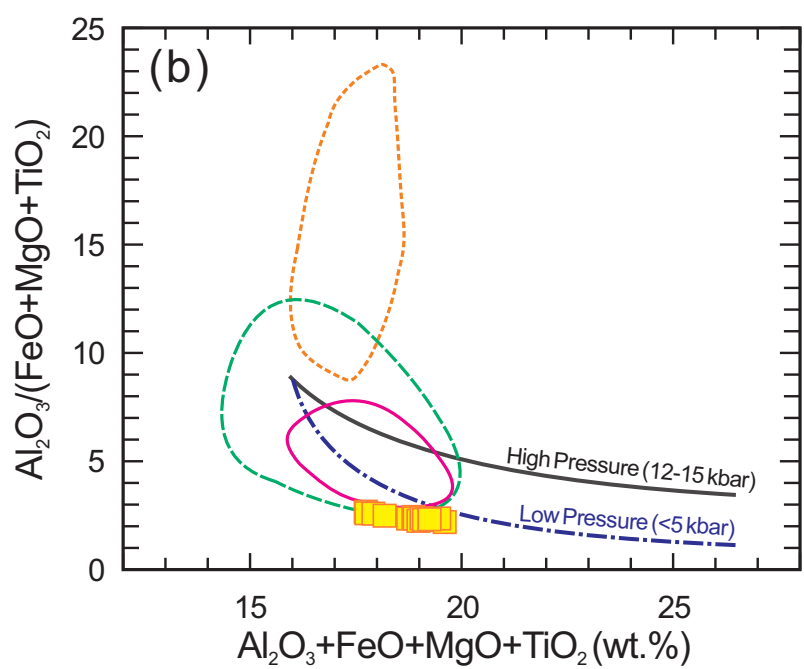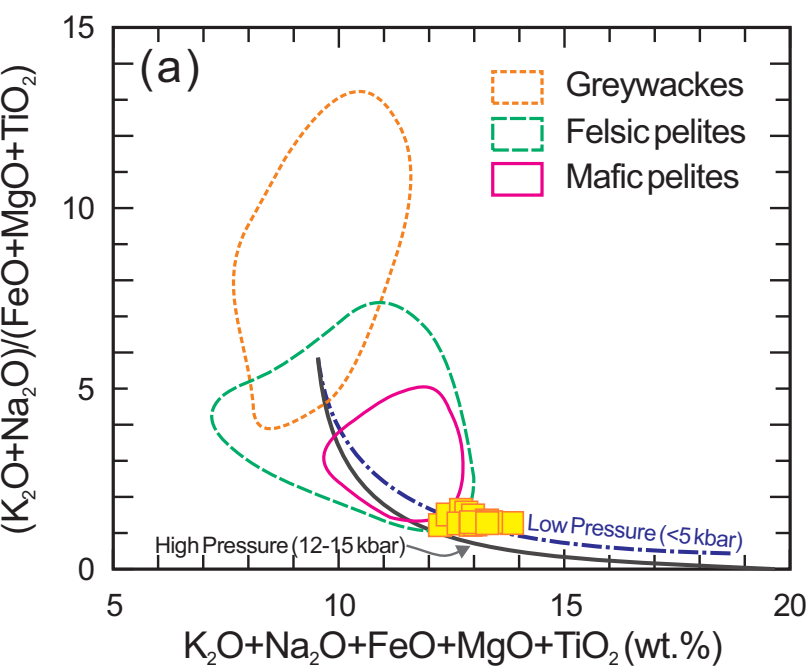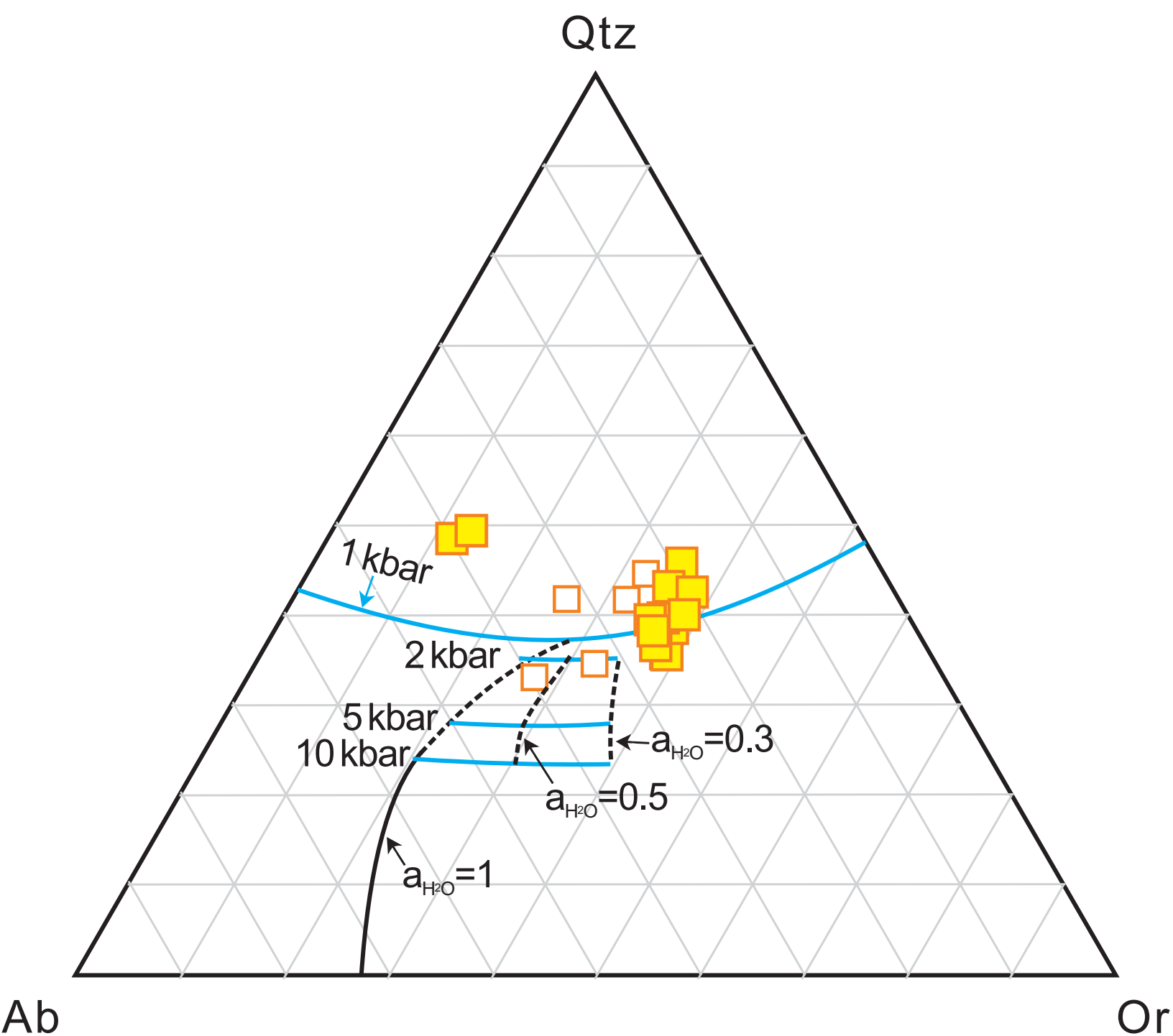|	09TB116-1	09TB116-4	09TB116-5	11SN17-1	11SN17-2	11SN18-1	11SN18-2	11SN19-1	11SN19-2	11SN19-3	11SN20-1	11SN20-2	11SN20-3
SiO_2	68.14	69.09	69.11	69.00	69.11	66.82	68.53	68.41	69.05	68.65	69.45	69.47	68.93
TiO_2	0.86	0.89	0.90	0.87	0.90	0.83	0.87	0.82	0.87	0.81	0.83	0.84	0.84
Al_2O_3	13.15	13.44	13.35	13.38	13.65	13.47	13.31	13.28	12.91	13.15	12.97	12.81	12.90
Fe_2O_3*	5.19	5.19	4.96	5.14	5.17	5.52	5.14	5.04	4.46	5.28	4.58	4.30	4.29
MnO	0.13	0.05	0.06	0.10	0.07	0.10	0.07	0.11	0.09	0.08	0.08	0.09	0.10
MgO	0.76	0.94	0.82	0.88	0.97	1.07	1.00	0.93	0.73	0.98	0.88	0.82	0.70
CaO	1.26	0.55	0.87	0.99	0.66	1.55	1.12	1.28	1.55	1.00	1.06	1.53	1.63
Na_2O	1.86	2.11	1.82	2.37	2.08	2.41	2.47	2.42	2.55	2.32	2.32	2.09	2.62
K_2O	5.21	5.01	4.90	5.23	5.12	5.30	5.09	4.92	5.27	5.13	5.44	5.38	5.26
P_2O_5	0.26	0.29	0.25	0.26	0.28	0.30	0.26	0.30	0.25	0.29	0.30	0.26	0.25
L.O.I	2.79	2.06	2.58	1.98	2.20	2.70	2.31	2.45	2.52	2.37	2.14	2.64	2.69
Total	99.60	99.63	99.62	100.19	100.22	100.07	100.17	99.95	100.23	100.06	100.05	100.23	100.22
A/CNK	1.20	1.36	1.35	1.18	1.34	1.08	1.15	1.14	1.02	1.18	1.11	1.06	1.00
$Mg^{\#}$	25.51	29.66	27.91	28.43	30.53	31.14	31.24	30.09	27.68	30.24	31.06	30.78	27.67
Sc	14.2	13.8	12.8	25.4	12.8	12.8	11.8	12.0	12.8	12.2	11.0	12.4	13.0
V	50.6	50.1	51.8	112	48.2	53.3	48.4	53.7	47.6	56.3	50.3	52.8	53.1
Cr	18.7	17.8	19.2	218	76.5	19.2	86.9	18	96	18.5	18.2	114.5	108.3
Co	32.0	29.9	30.9	14.2	7.93	9.35	7.75	5.74	7.39	6.87	6.45	7.91	7.27
Ni	11.7	9.62	11.2	28.5	13.2	9.9	16.7	8.7	15.0	8.60	8.72	15.29	14.52
Ga	18.6	20.2	18.9	42.5	18.9	19.9	18.9	19.6	18.4	18.8	18.2	16.3	16.6
Rb	169	169	160	371	182	180	178	182	182	184	174	166	170
Sr	131	136	134	200	91.6	97	113	133.3	111.8	118.2	69	94	96.9
Y	52.8	53.2	48.9	105	48.4	52.2	46.2	53.2	47.6	53.7	51.5	46.8	47.5

Zr	368	408	341	1141	448	349	400	358	489	340	407	422	439
Nb	23.6	23.7	22.7	45.6	21.9	26.0	21.7	25.2	21.0	25.0	25.5	21.1	21.3
Cs	2.77	1.74	2.44	3.60	1.54	1.50	1.64	2.09	1.60	1.75	1.01	1.13	1.18
Ba	1169	1200	1365	2332	895	867	853	954	1002	947	950	960	967
La	85.7	88.1	83.1	176	83.0	78.0	78.6	85.1	82.2	84.7	82.6	76.9	77.7
Ce	177	184	170	359	167	155	155	167	165	170	168	157	160
Pr	22.1	23.0	20.5	42.2	20.1	18.6	18.9	20.0	19.6	20.7	20.4	18.6	18.8
Nd	76.6	80.8	71.8	162.1	77.7	71.0	72.6	78.2	75.9	79.5	77.7	71.7	73.2
Sm	14.1	15.2	13.0	29.3	14.3	13.1	13.3	13.8	13.6	14.3	13.9	13.1	13.0
Eu	2.80	2.56	1.99	4.79	2.62	2.24	2.38	2.31	2.44	2.71	2.31	2.44	2.47
Gd	12.2	13.1	10.9	25.9	12.5	11.7	11.5	12.0	12.2	12.7	12.2	11.7	11.9
Tb	1.79	1.91	1.60	3.71	1.78	1.64	1.68	1.66	1.76	1.80	1.65	1.66	1.67
Dy	9.61	10.11	8.66	20.2	9.59	9.47	9.18	9.25	9.69	9.64	9.32	9.02	9.06
Ho	1.91	1.98	1.72	4.00	1.82	1.85	1.80	1.85	1.90	1.92	1.82	1.80	1.79
Er	5.25	5.26	4.79	10.7	5.03	4.83	4.75	4.83	4.96	4.92	4.72	4.94	4.93
Tm	0.75	0.80	0.69	1.56	0.74	0.70	0.69	0.70	0.74	0.71	0.68	0.70	0.71
Yb	4.92	5.23	4.67	10.1	4.88	4.47	4.45	4.46	4.74	4.45	4.37	4.68	4.65
Lu	0.74	0.78	0.70	1.56	0.77	0.67	0.69	0.68	0.73	0.67	0.66	0.75	0.73
Hf	10.0	11.0	9.49	28.4	11.6	9.7	10.3	9.7	12.4	9.29	10.87	10.84	11.1
Ta	2.07	2.16	2.04	3.74	1.82	1.84	1.75	1.84	1.74	1.81	1.81	1.70	1.74
Pb	20.2	22.1	17.7	40.2	20.2	18.8	21.9	18.8	19.0	15.3	17.0	20.9	21.2
Th	34.8	36.0	33.6	73.4	34.0	35.0	33.8	34.4	35.0	34.4	34.9	33.1	33.3
U	4.72	5.00	4.81	10.3	4.72	4.81	4.79	4.80	4.68	4.63	4.34	4.55	4.57
T_{Zr} (°C)	878	902	883	1004	910	856	880	868	887	867	880	879	873
Ga/Al	2.67	2.84	2.67	6.00	2.61	2.80	2.68	2.79	2.70	2.71	2.65	2.41	2.43

Fe_2O_3* = Total Fe_2O_3 content; $Mg^{\#}$ = Mg^{2+}/(Mg^{2+}+Fe^{2+})×100; A/CNK = molecular Al_2O_3/(CaO+Na_2O+K_2O); T_{Zr} are calculated after Watson and Harrison (1983).

Table 2 Sr and Nd isotope data for the Comei granites

Sample	Rb (ppm)	Sr (ppm)	Sm (ppm)	Nd (ppm)	^{87}Rb/^{86}Sr	^{87}Sr/^{86}Sr	(^{87}Sr/^{86}Sr)$_i$	^{147}Sm/^{144}Nd	^{143}Nd/^{144}Nd	(^{143}Nd/^{144}Nd)$_i$	$\varepsilon_{Nd}(t)$	T_{Nd}^{DM} (Ma)	$f_{Sm/Nd}$
11SN16-1	77.4	68.1	12.6	67.6	3.29	0.730404±6	0.7238	0.113	0.511917±3	0.511814	-12.6	1870	-0.42
11SN17-1	371	200	29.3	162	5.38	0.736446±6	0.7257	0.110	0.511904±3	0.511804	-12.8	1831	-0.44
11SN18-2	178	113	13.3	72.6	4.57	0.735865±5	0.7268	0.111	0.511906±3	0.511805	-12.8	1851	-0.43
11SN19-2	182	112	13.6	75.9	4.72	0.735519±6	0.7261	0.109	0.511910±4	0.511811	-12.6	1805	-0.45
11SN20-2	166	94.3	13.1	71.7	5.10	0.735452±6	0.7253	0.111	0.511905±3	0.511803	-12.8	1856	-0.43
09TB116-1	169	131	14.1	76.6	3.74	0.736342±16	0.7289	0.112	0.511930±8	0.511828	-12.3	1826	-0.43
09TB116-4	169	136	15.2	80.8	3.62	0.736694±13	0.7295	0.114	0.511936±9	0.511832	-12.2	1856	-0.42
09TB116-5	160	134	13.0	71.8	3.46	0.735685±15	0.7288	0.110	0.511943±8	0.511843	-12.0	1781	-0.44

^{87}Rb/^{86}Sr and ^{147}Sm/^{144}Nd are calculated using whole-rock Rb, Sr, Sm and Nd contents in Table 1.

$\varepsilon_{Nd}(t) = [(^{143}Nd/^{144}Nd)s/(^{143}Nd/^{144}Nd)_{CHUR}-1] \times 10000$. $T_{DM} = \ln[^{143}Nd/^{144}Nd - (^{143}Nd/^{144}Nd)_{DM}] / [^{143}Sm/^{144}Nd - (^{147}Sm/^{144}Nd)_{DM}] / \lambda$ (DePaolo, 1988).

In the calculation, $(^{143}Nd/^{144}Nd)_{CHUR}=0.512638$, $(^{147}Sm/^{144}Nd)_{CHUR}=0.1967$, $(^{143}Nd/^{144}Nd)_{DM}=0.513151$, $(^{147}Sm/^{144}Nd)_{DM}=0.2135$, $(^{147}Sm/^{144}Nd)_{CC}=0.12$, $\lambda_{Sm}=6.54 \times 10^{-12}$/yr and t=140 Ma.

Background dataset for online publication only